Excitation spectra of the Ce monopnictides within dynamical mean-field theory

J. Lægsgaard and A. Svane
Institute of Physics and Astronomy, University of Aarhus, DK-8000 Aarhus C, Denmark
(Received 29 June 1998)

The excitation spectra of the Ce monopnictides CeN, CeP, and CeAs are calculated using a lattice tight-binding model including the local Coulomb repulsion U on the Ce $4f$ orbitals. The model is treated within the dynamical mean-field theory, whereby the problem is mapped onto an effective Anderson impurity model. This is solved in a finite-U extension of the noncrossing approximation, including lowest-order crossing diagrams. The lattice model is parametrized by means of *ab initio* calculations. The calculated spectra are in good agreement with experiment. In particular, dispersive quasiparticle peak positions are found close to the Fermi edge in CeP. CeN shows metallic Fermi-liquid behavior with a correlation-induced mass enhancement factor of ~ 5 around the Fermi level. [S0163-1829(98)09843-9]

I. INTRODUCTION

The study of heavy fermion (HF) and related systems has been a major research area in condensed-matter physics for more than 20 years.[1] Briefly speaking, the HF phase may be characterized as a paramagnetic Fermi-liquid-like state, with an anomalously large density of states around the Fermi level, leading to extreme values for quantities like the magnetic susceptibility and electronic specific heat, corresponding to effective quasiparticle masses of 10–1000 times the free-electron mass. Furthermore, the spectral features of the systems (as measured in, e.g., photoemission or inverse photoemission spectroscopy) are poorly described by single-particle theory on a broad energy scale, and even the narrow set of quasiparticlelike states around the Fermi level cannot in general be described by a parameter-free band theory, although the Fermi surface topologies measured in de Haas–van Alphen experiments are often well reproduced by band-structure calculations.[2] The HF phase appears in compound systems containing Ce, Yb, U, or Pu ions, and it is generally accepted that the phenomenon is connected to the strong local Coulomb repulsions in the narrow valence-f orbitals of these ions. The stoichiometries of the HF compounds are often very complicated, and this is also true of the phase diagrams as a function of composition, temperature, pressure, etc. The HF phases are usually found at low temperatures and often in competition with phases exhibiting more conventional band structures, or different patterns of magnetic order. Despite a large research effort, the understanding of these phase diagrams is still far from complete.

One of the most successful phenomenological models of the HF phase has for the past 15 years been the single-impurity Anderson model,[3–5] in which a single multiplet of f orbitals with strong local Coulomb repulsion is treated like an impurity residing in a metallic host. The basic parameters of this model are the hybridization strengths between the conduction and impurity states, and the position of the impurity levels relative to the Fermi level of the medium. Models of this kind have explained the origin of the heavy quasiparticles as well as the unusual spectral features, and have also been able to place the HF phase in a broader context, as an intermediate case between a localized behavior, where the f multiplet is not interacting with the surroundings, but has a fixed integral occupation number, and the mixed-valence case where the f occupation is far from integral, the ion fluctuating between two different configurations. The use of Anderson impurity models is, however, still controversial for several reasons: First, many HF systems show dispersion effects in photoemission and other optical experiments, also for the HF states, which indicates interatomic interaction, at variance with the assumption of isolated impurities.[6–8] This is particularly evident as one goes towards the mixed-valence regime, but has also been observed in several compounds that are unmistakably HF-like.[7] Second, attempts to parametrize impurity models by *ab initio* calculations have met with mixed success. On one hand, band-structure calculations of the hybridization strengths have been able to explain trends with composition and pressure of the HF compounds,[9,10] but on the other hand, quantitative comparisons to experimental results have usually not been possible without the introduction of overall rescaling parameters for the hybridization strengths.[9,11] Additionally, no reliable *ab initio* scheme has been found for the calculation of the bare impurity level positions. Thirdly, the theoretical foundation and range of validity of the impurity approximation to the true lattice problem is not clear.

A recent theoretical advance in the understanding of electron systems with strong local correlations has been the realization, that the assumption of a **k**-independent self-energy operator (known as the ''local approximation''[12]) allows for a mapping of a lattice problem onto an effective impurity model.[13,14] This approach is commonly referred to as the ''dynamical mean-field theory'' (DMFT). The parameters of the impurity model depend on the interacting lattice Green's function, so the problem has to be solved by a self-consistency procedure. At self-consistency, the local Green's function of the lattice model equals the Green's function of the effective impurity problem. In this way, the phenomenological impurity models may be reinterpreted as representing solutions for the local Green's function of a lattice problem in the local approximation. This picture still allows for the presence of dispersion effects in the **k**-resolved spectra, (caused by dispersion effects in the single-particle part of the Hamiltonian), thus removing a major point of criticism against the impurity model. Furthermore, the fact that the hybridization strength should be determined as that of a cor-

related medium could be part of the explanation why the attempts of *ab initio* calculations of these quantities have not in general been successful. The local approximation can be justified in infinite spatial dimensions,[15] and there are indications that it is reasonably accurate also for close-packed three-dimensional structures,[16,17] but a quantitative estimate of the error terms is not known in general.

From the preceding discussion it is clear that a natural step forward in HF research would be to replace the single-impurity model by a lattice model within the local approximation, and solve it by the well-established methods for handling impurity problems in the HF regime. Up to now, DMFT studies have mostly been done for simple models with a small number of orbitals.[13,18] Recently, Anisimov and co-workers[19] have presented DMFT calculations for $La_{1-x}Sr_xTiO_3$, using a modified perturbation scheme,[18] incorporated into the LMTO band-structure formalism. The purpose of the present project is to extend DMFT studies into the HF regime, by using a self-energy functional appropriate to the description of such systems, together with a multiorbital tight-binding model. Our goal is twofold: First, we want to explore the elementary properties of such a model, most importantly the behavior of the hybridization function as one proceeds towards self-consistency and the possible dispersion effects arising in the heavy-electron states. Second, we want to investigate the possibility of parametrizing such a model directly from *ab initio* calculations to obtain quantitative predictions for a realistic system. As a specific example, we have chosen the Cerium monopnictide systems CeN, CeP, and CeAs. This choice is partly motivated by the fact that these systems are fairly simple, and can be described by a limited basis set, and partly that they show an interesting behavior in several ways. First, there is a pronounced variation of the physical properties with chemical composition in these compounds.[20,21] While CeN tends towards the mixed-valence region,[22–25] the rest of the series show semimetallic behavior,[20] yet with pronounced hybridization effects in the excitation spectra.[6,26,23] The study of this series of compounds will therefore probe the ability of our model to describe different parameter regimes. Second, the semimetallic gap in the density of states of the weakly correlated states surrounding the *f* levels in CeP and CeAs implies that these systems are particularly sensitive to the changes in the effective hybridization function arising from the onset of correlations. Third, the photoemission spectra of the Ce monopnictides show dispersion effects not contained in the single-impurity model.[6]

The remainder of the paper is organized as follows: In Sec. II, the basic ideas of the theoretical approach are introduced, and most of the necessary formalism is developed. A detailed derivation of the solution method for the impurity problem is, however, deferred to the Appendix. In Sec. III our numerical results are presented and discussed. Finally, we present our conclusions and prospects for future work in Sec. IV.

II. FORMAL THEORY

A. Basic definitions

Most present-day studies of strongly correlated electron systems are based on tight-binding Hamiltonians with local Coulomb repulsions, i.e., models of the generic form

$$\hat{H}=\sum_{mm'\mathbf{R}\mathbf{R}'} T^{mm'}_{\mathbf{R}\mathbf{R}'}\hat{\Psi}^{\dagger}_{m\mathbf{R}}\hat{\Psi}_{m'\mathbf{R}'} + \sum_{\mathbf{R}m_{1-4}} U^{m_1m_2}_{m_3m_4}\hat{\Psi}^{\dagger}_{m_1\mathbf{R}}\hat{\Psi}^{\dagger}_{m_2\mathbf{R}}\hat{\Psi}_{m_3\mathbf{R}}\hat{\Psi}_{m_4\mathbf{R}}. \quad (1)$$

Here the vectors $\mathbf{R}$ denote points on a Bravais lattice, and the operators $\hat{\Psi}_{m\mathbf{R}},\hat{\Psi}^{\dagger}_{m\mathbf{R}}$ are destruction and creation operators for electrons in the state m centered on the Bravais lattice site $\mathbf{R}$. In the case of a lattice with a polyatomic basis, the summation over m would include summation over the basis vectors. The T and U parameters are one- and two-body matrix elements describing the chemical nature of the orbitals. Assuming translational invariance of the matrix elements one can transform to a $\mathbf{k}$-space representation:

$$\hat{\Psi}_{m\mathbf{k}}=\frac{1}{\sqrt{N}}\sum_{\mathbf{R}} e^{i\mathbf{k}\cdot\mathbf{R}}\hat{\Psi}_{m\mathbf{R}}, \quad (2)$$

$$\hat{H}=\sum_{mm'\mathbf{k}} T^{mm'}_{\mathbf{k}}\hat{\Psi}^{\dagger}_{m\mathbf{k}}\hat{\Psi}_{m'\mathbf{k}} + \frac{1}{N}\sum_{\mathbf{k}\mathbf{k}'\mathbf{p}}\sum_{m_{1-4}} U^{m_1m_2}_{m_3m_4}\hat{\Psi}^{\dagger}_{m_1\mathbf{k}}\hat{\Psi}^{\dagger}_{m_2\mathbf{k}'}\hat{\Psi}_{m_3\mathbf{k}+\mathbf{p}}\hat{\Psi}_{m_4\mathbf{k}'-\mathbf{p}}, \quad (3)$$

with N denoting the total number of primitive cells in the crystal. To calculate dynamical properties of a many-particle system one needs to evaluate one- and two-particle Green's functions. In this work, we shall focus on the one-particle Green's function, which is defined by

$$G_{mm'\mathbf{k}}(t)=-i\langle\hat{T}\hat{\Psi}^{\dagger}_{m\mathbf{k}}(t)\hat{\Psi}_{m'\mathbf{k}}(0)\rangle, \quad (4)$$

$$\hat{\Psi}_{m\mathbf{k}}(t)=e^{i\hat{H}t}\hat{\Psi}_{m\mathbf{k}}e^{-i\hat{H}t}. \quad (5)$$

The operator $\hat{T}$ is the usual time-ordering operator that orders the time-dependent fermion operators with the earliest times to the right. The brackets denote a thermal average. Time translational invariance is assumed, so that it is only necessary to calculate the Green's function of one time variable. In frequency space, the Green's function can be expressed as[27]

$$G_{mm'\mathbf{k}}(\omega)\equiv\int dt e^{i\omega t}G_{mm'\mathbf{k}}(t)=\int d\varepsilon\frac{\rho_{mm'\mathbf{k}}(\varepsilon)}{\omega-\varepsilon}, \quad (6)$$

$$\rho_{mm'\mathbf{k}}(\varepsilon)=\sum_{\lambda\lambda'}\frac{e^{-\beta(E_\lambda-\mu)}}{Z}[\langle\lambda|\hat{\Psi}^{\dagger}_{m\mathbf{k}}|\lambda'\rangle \times\langle\lambda'|\hat{\Psi}_{m'\mathbf{k}}|\lambda\rangle\delta(\varepsilon-(E_{\lambda'}-E_\lambda)) +\langle\lambda|\hat{\Psi}_{m'\mathbf{k}}|\lambda'\rangle\langle\lambda'|\hat{\Psi}^{\dagger}_{m\mathbf{k}}|\lambda\rangle \times\delta(\varepsilon-(E_\lambda-E_{\lambda'}))] \quad (7)$$

The states $|\lambda\rangle$ are eigenstates of the many-particle system, $\beta=1/k_BT$, μ is the chemical potential, and Z is the partition function in the grand canonical ensemble. For the Fourier transform to be well defined, the variable ω must carry an infinitesimal imaginary part the sign of which follows the sign of the real part. The functions $\rho_{mm'}$ are the spectral

functions, and can be measured (if the variation in dipole matrix elements between initial and final states is assumed unimportant) in photoemission/inverse photoemission experiments. In the remainder of this paper we shall adopt the matrix notation

$$G_{mm'\mathbf{k}}(\omega) \equiv [\bar{\bar{G}}_{\mathbf{k}}(\omega)]_{mm'}. \tag{8}$$

The unperturbed Green's function, i.e., the Green's function obtained by keeping only the one-particle terms in the Hamiltonian, is denoted by $\bar{\bar{G}}_{0\mathbf{k}}(\omega)$, and the self-energy matrix is defined by

$$\bar{\bar{\Sigma}}_{\mathbf{k}}(\omega) = \bar{\bar{G}}_{0\mathbf{k}}(\omega)^{-1} - \bar{\bar{G}}_{\mathbf{k}}(\omega)^{-1}. \tag{9}$$

Once the single-particle part of the problem is solved, determination of the full Green's function is equivalent to determination of the self-energy.

B. Local approximation

The equations for the self-energy derived within many-body theory are usually too complicated to be solvable without approximations. In recent years, the so-called local approximation has proved to be a very fruitful approach for model systems of the kind described above.[14,12,28,29] The approximation consists of neglecting the **k** dependence of the self-energy matrix, so that the real-space self-energy becomes a local quantity. The simplifications arising from this assumption are twofold: First, the self-energy is reduced from a four-dimensional to a one-dimensional object, which is in itself of some importance for practical calculations. The most important implication is, however, that locality of the self-energy allows for a mapping from the lattice problem to an effective impurity problem of the form[13]

$$\hat{H}^{imp} = \sum_{\lambda} \varepsilon_{\lambda} \hat{c}_{\lambda}^{\dagger} \hat{c}_{\lambda} + \sum_{\lambda m} (V_{m\lambda} \hat{c}_{\lambda}^{\dagger} \hat{c}_{m} + \text{H.c.}) + \sum_{m} \varepsilon_{m} \hat{c}_{m}^{\dagger} \hat{c}_{m} + \sum_{m_{1-4}} U_{m_3 m_4}^{m_1 m_2} \hat{c}_{m_1}^{\dagger} \hat{c}_{m_2}^{\dagger} \hat{c}_{m_3} \hat{c}_{m_4}. \tag{10}$$

Here the quantum numbers λ denote states of an unspecified medium, while m denotes states of the impurity. The U parameters are the same as in the original problem, while the energies ε_m may differ. The parameters of the effective impurity model are determined from the condition that the unperturbed single-particle Green's function of this model should be given by

$$\bar{\bar{G}}_{0imp}(\omega) = [\bar{\bar{G}}_{loc}^{-1}(\omega) + \bar{\bar{\Sigma}}(\omega)]^{-1}, \tag{11}$$

where $\bar{\bar{G}}_{loc}$ is the local lattice Green's function in real space, i.e.,

$$\bar{\bar{G}}_{loc}(\omega) = \frac{1}{N} \sum_{\mathbf{k}} \bar{\bar{G}}_{\mathbf{k}}(\omega). \tag{12}$$

If one is able to solve the effective impurity model, i.e., to calculate to some accuracy the interacting impurity Green's function, $\bar{\bar{G}}_{imp}(\omega)$, the self-energy of the lattice problem in turn may be obtained as

$$\bar{\bar{\Sigma}}(\omega) = \bar{\bar{G}}_{0imp}^{-1}(\omega) - \bar{\bar{G}}_{imp}^{-1}(\omega). \tag{13}$$

Since determination of the impurity model parameters requires knowledge of the interacting lattice Green's function $\bar{\bar{G}}_{loc}(\omega)$, which depends on $\bar{\bar{\Sigma}}(\omega)$, Eqs. (11)–(13) constitute a self-consistency problem. Inserting Eq. (13) into Eq. (11), it is seen that one way of formulating the self-consistency requirement is to demand equality of the lattice and impurity Green's functions. Thus, within the local approximation, any quantity that only depends on the local Green's function (e.g., results of angle-integrated spectroscopies) can be determined by solving a suitable impurity problem. The computational steps in the self-consistency procedure are straightforward (although numerically tedious), so that the nontrivial problem that remains is the solution of the single-impurity model. This problem is, however, much better understood than the corresponding lattice models. Therefore, the existence of the above connection is definitely a step forward.

Assessing the validity of the local approximation is not a straightforward matter. It is trivially justified in the narrow-band limit, since all dispersion effects disappear, and less trivially in the limit of infinite spatial dimension (that is, infinite coordination number).[15] Most applications of the method described above have up to now been concerned with exact solution of infinite-dimensional lattice models.[14,13,18] In finite dimensions the validity of the local approximation has been studied in the weak-coupling limit by second-order perturbation theory,[16] and it has been found that the error in the self-energy is less than 10% for three-dimensional lattices, and that the spectral functions calculated with and without the local approximation are almost identical. For systems of lower dimensionality than 3, the approximation appears to be less adequate in the limit of weak interaction. A study of an intermediate-interaction case (the magnitude of U being comparable to the bandwidth) in a one-dimensional ferromagnetic Hubbard model using a three-body scattering approach showed that the local approximation gave a fairly accurate description of the angle-integrated (i.e., local) spectral function.[29]

C. Model

The cerium monopnictides CeM (M=N,P,As, . . .) constitute a class of systems showing strong correlation-induced enhancements of electronic effective masses,[20,22] although they are not usually referred to as heavy-fermion materials. At ambient conditions, these compounds have the NaCl crystal structure. To set up a simple tight-binding model for the single-particle Hamiltonian of these compounds, we choose a minimal basis set consisting of Ce *df* orbitals, and M *p* orbitals. The M *s* and Ce *sp* orbitals are excluded since they are either very low (M *s* and Ce 5*p*) or very high (Ce 6*sp*) in energy. To further simplify the problem spin-orbit coupling is neglected, and we assume that only the Γ_{15} multiplet of the Ce-*f* states needs to be considered. The reason for the latter assumption is that only the Γ_{15} states are coupled to the *p* lobes pointing directly towards a given Ce atom when the M *p* orbitals are written in the cubic harmonic representation. We emphasize that these approximations are mainly made for calculational convenience. In reality the spin-orbit split-

ting of the Ce f states is much larger (approximately 0.25 eV) than the splittings arising from crystal fields, so a more realistic procedure would be to restrict the Ce f states to only the $j=\frac{5}{2}$ multiplet. This would, however, lead to a mixing of the spin channels, thus doubling the size of the Hamiltonian matrix. As it turns out, the density of states (DOS) of the Ce monopnictides is reasonably well described by the nonrelativistic Hamiltonian, and for the many-body calculations the difference is not so important, since the degeneracy of the Γ_{15} multiplet is identical with the number of $j=\frac{5}{2}$ states (the importance of the degeneracy is discussed in the Appendix). The precise orbital character of the Ce f states becomes important when one wants to study crystal-field splitting effects, but this issue is not addressed in the present work.

The band structure of the tight-binding model described above can be parametrized in terms of Slater-Koster two-center integrals.[30] A relatively small number of these parameters have been adjusted to match the results of *ab initio* band-structure calculations, as described in Sec. II E. In addition, an appropriate choice for the two-body part of the Hamiltonian has to be made. In the present work, we shall only consider the simplest possible choice, namely, an on-site f-f repulsion term U. Other terms of interest could be the f-d or the d-d Coulomb interactions, but their inclusion would complicate the self-energy calculation and is therefore left for future work. The complete lattice Hamiltonian may now be written as

$$\hat{H}=\sum_{\mathbf{k}\sigma}(\hat{H}^{(c)}_{\mathbf{k}\sigma}+\hat{H}^{(cf)}_{\mathbf{k}\sigma}) + \sum_{\mathbf{R}}\left(\varepsilon^f\hat{n}^f_{\mathbf{R}\sigma}+U\sum_{\nu\nu'\sigma'}\hat{n}^f_{\mathbf{R}\nu\sigma}\hat{n}^f_{\mathbf{R}\nu'\sigma'}\right), \tag{14}$$

$$\hat{H}^{(c)}_{\mathbf{k}\sigma}=\sum_{\nu}\varepsilon^p_{\mathbf{k}\nu}\hat{p}^\dagger_{\mathbf{k}\nu\sigma}\hat{p}_{\mathbf{k}\nu\sigma}+\sum_{\mu'}\varepsilon^d_{\mathbf{k}\mu'\sigma}\hat{d}^\dagger_{\mathbf{k}\mu'\sigma}\hat{d}_{\mathbf{k}\mu'\sigma} + \sum_{\nu\neq\nu'}t^{\nu\nu'}_{\mathbf{k}}\hat{p}^\dagger_{\mathbf{k}\nu\sigma}\hat{p}_{\mathbf{k}\nu'\sigma}+\sum_{\mu\neq\mu}t^{\mu\mu'}_{\mathbf{k}}\hat{d}^\dagger_{\mathbf{k}\mu\sigma}\hat{d}_{\mathbf{k}\mu'\sigma} + \sum_{\nu\mu'}(t^{\nu\mu'}_{\mathbf{k}}\hat{p}^\dagger_{\mathbf{k}\nu\sigma}\hat{d}_{\mathbf{k}\mu'\sigma}+\text{H.c.}), \tag{15}$$

$$\hat{H}^{cf}_{\mathbf{k}\sigma}=\sum_{\nu}\delta_{\mathbf{k}\nu}\hat{p}^\dagger_{\mathbf{k}\nu\sigma}\hat{f}_{\mathbf{k}\nu\sigma}+\sum_{\nu\mu'}\delta'_{\mathbf{k}\nu\mu'}\hat{d}^\dagger_{\mathbf{k}\mu'\sigma}\hat{f}_{\mathbf{k}\nu\sigma}+\text{H.c.}, \tag{16}$$

with the operators $\hat{p},\hat{d},\hat{f}$ being destruction operators for M-p, Ce-d, and Ce-f electrons, respectively.

D. Self-energy functional

Having set up the model, our next step is to choose an approximation for the self-energy functional. To this end, we shall rewrite the effective impurity problem in the form[4]

$$\hat{H}_{imp}=\sum_{\nu}\int d\varepsilon[\varepsilon\hat{c}^\dagger_{\nu\varepsilon}\hat{c}_{\nu\varepsilon}+(V(\varepsilon)\hat{c}^\dagger_{\nu\varepsilon}\hat{f}_\nu+\text{H.c.})] + \varepsilon_f\sum_{\nu}\hat{n}^f_\nu+U\sum_{\nu'>\nu}\hat{n}^f_\nu\hat{n}^f_{\nu'}. \tag{17}$$

The operators $\hat{c}_{\nu\varepsilon}$ are destruction operators for a set of band states of energy ε and symmetry (including spin) ν, while the operators $\hat{f}_\nu$ are destruction operators for effective impurity (f) states with energy ε_f and mutual Coulomb repulsion U, and the operators $\hat{n}^f_\nu$ are the number operators for the f states. Suppressing the symmetry index (since our model contains only one irreducible f representation), the single-particle f Green's function of this model is given by

$$G^f_0(\omega)=\frac{1}{\omega-\varepsilon_f-\int d\varepsilon\dfrac{|V(\varepsilon)|^2}{\omega-\varepsilon}}. \tag{18}$$

The impurity Green's function is a diagonal matrix, since we have only included one of the irreducible f-state representations. It then follows by comparison of Eqs. (11) and (18) that

$$|V(\varepsilon)|^2=\frac{1}{\pi}\,\text{Im}([G_{loc}(\varepsilon)]^{-1}_f+\Sigma(\varepsilon))\text{sgn}(\varepsilon). \tag{19}$$

For simplicity, we take the ε_f-level position of the impurity problem to be identical to that of the lattice Hamiltonian. An alternative (more rigorous) procedure would be to take the impurity f level as the average of the quantity

$$\varepsilon_f(\omega)=\omega-P\int d\varepsilon\frac{|V(\varepsilon)|^2}{\omega-\varepsilon}-[G_{loc}(\omega)]^{-1}_f-\Sigma(\omega). \tag{20}$$

In practice we have found that the two procedures lead to identical results.

A common approximation adopted for solving the impurity problem in the regime of weak hybridization and large orbital degeneracy of the impurity states is the so-called non-crossing approximation (NCA).[5] In this approach, the U parameter is taken to be infinite, and the Green's function is determined in terms of resolvent operators, which can be expanded in powers of the hybridization strength. The NCA corresponds to the summation of a particular subset of the resulting series, and is believed to give a good description of the $U=\infty$ impurity model at temperatures above a (very small) ''pathology scale.'' Theories based on NCA solutions of infinite-U impurity models have been very successful as phenomenological descriptions of HF and related systems.[5,10]

In the present work we need to go beyond the $U=\infty$ approximation for two reasons: First, to perform the self-consistency procedure described in Sec. II B, we need to determine a self-energy from the solution of the impurity problem. This can be done by the following formula:

$$\Sigma(\omega)=\omega-\varepsilon_f-\int d\varepsilon\frac{|V(\varepsilon)|^2}{\omega-\varepsilon}-\left(\int d\varepsilon\frac{\rho^{imp}(\omega)}{\omega-\varepsilon}\right)^{-1}, \tag{21}$$

where ρ^{imp} is the (many-body) spectral function of the impurity model. To get the correct asymptotic behavior of the self-energy, it is important, that ρ^{imp} is properly normalized, and since most of the spectral weight in the heavy-fermion regime resides in a set of states high above the Fermi level corresponding to f^1-f^2 absorption processes, it is important

to include the f^2 states in some way. Secondly, the $U=\infty$ approximation is not very well justified for the parameter regime that is relevant for our study, as will be discussed later, and this is probably the case for most physical systems. The success of the NCA as a phenomenological theory must be ascribed to the fact that the theory gives a correct qualitative description of heavy-fermion physics, so that finite-U effects can be absorbed in one or more adjustable parameters. Since we want to investigate the feasibility of *ab initio* parametrization, we need to take these effects explicitly into account.

The inclusion of finite-U effects in an NCA-like theory has been discussed by Pruschke and Grewe.[31] From the analytical point of view it is a straightforward matter, but it entails certain numerical difficulties. We have devised a relatively simple and fast approximation scheme that appears to work well for the cases under study here. The scheme is discussed in the Appendix. Basically, it exploits the fact that most of the spectral weight of the doubly occupied f configurations is well separated in energy from the rest of the f spectrum.

E. Parametrization scheme

To parametrize the tight-binding lattice model of the Ce monopnictides described in Sec. II C, we have performed band-structure calculations for these compounds using the local density approximation (LDA) to density-functional theory.[32] Experience shows that the band structures obtained in this way give a good description of the elementary excitation spectrum of wide-band electron systems. The calculations were done using linear muffin-tin orbitals[33,34] (LMTO's) in the atomic-spheres approximation (ASA). This method divides the space into volume-filling spheres centered around the points of the crystal lattice, and neglects the interstitial and overlap regions. Within each sphere, the potential and charge density are spherically symmetrized, and the wave functions are expanded in eigenfunctions of the symmetrized potential, and their derivatives with respect to the eigenenergies (the so-called ϕ and $\dot{\phi}$ functions). From these functions, which are restricted to a particular atomic sphere, a set of localized continuous and differentiable basis functions (denoted χ) are constructed. They retain the definite angular momentum character with respect to the central site, but do not, in general, constitute an orthonormal basis set. The scalar relativistic approximation[34] (which neglects spin-orbit coupling) is invoked, and a minimal basis set with only one ϕ function for each angular momentum quantum number is used. While this cannot be said to be a state-of-the-art treatment of the Ce monopnictides, it is accurate enough to capture the essential variation of hybridization strength and DOS topology with chemical composition. At the same time, the LMTO basis set is easily related to simpler tight-binding models of the sort described above, in Sec. II C.

The parametrization of the tight-binding model from the LMTO calculations is done by first fixing the relative positions of the *pdf*-energy levels to match the values of the LMTO ''band-center parameters.'' To determine the various hybridization terms, we extract a Ce 4*f*-projected DOS and determine an effective hybridization function from Eq. (19), with the self-energy set to zero, which is then to be matched by the corresponding function obtained from the tight-binding model. Having fixed these parameters, we need to determine the local Coulomb repulsion U and, more importantly, it is essential for our self-energy calculation to know the *bare* f-level position. It is not at all clear how this is related to the f energy obtained from the band-structure calculation.

To address these questions, we shall interpret the tight-binding energy levels on a particular atom as representing the energy cost of moving an electron on that atom from one orbital to another, including intra-atomic relaxation effects, but excluding effects of hybridization. This implies that we can extract the value of U, as well as the difference between the Ce f and d levels by evaluating total-energy differences between free atoms in various configurations. To mimic the screening effects in the solid, and to have consistency in our parametrization procedure, we shall do the atomic calculation by means of the local spin-density approximation (LSDA). Since it is not clear whether the screening effects in the region of the 4*f* states are well described by the LSDA, we shall also investigate the effect of treating these states within the self-interaction corrected local-spin-density approximation (SIC-LSDA).[35] In this approach, the 4*f* self-interaction terms in the Hartree and exchange-correlation parts of the LSDA energy functional are explicitly subtracted, leading to an improved description of the Coulomb interactions within the 4*f* shell. As we shall see, the tight-binding model with parameters extracted using the SIC-LSDA appear to give better agreement with the experimental data.

Having obtained an atomic value for the difference between f and d energies, we shift the position of the tight-binding f level relative to the others to match this value, keeping the separation between the Ce-d and M-p levels fixed. We are thus assuming, that the relative positions of these levels are well described by the band-structure calculation. This completes the parametrization of our model. All parameters have essentially been determined by results of *ab initio* theory, so our results will be a critical test of the ability of LDA-like methods to describe the elementary properties of Ce systems.

III. NUMERICAL RESULTS AND DISCUSSION

A. *Ab initio* parametrization

1. LMTO calculations

To describe the elementary excitations of the weakly correlated electron gas surrounding the Ce f electrons, we have performed band-structure calculations for CeN, CeP, and CeAs in the NaCl crystal structure, at the experimentally determined lattice constants.[36] In all cases, we worked in a single energy panel, with only one set of basis functions per angular momentum channel. This makes the description of the Ce p states a delicate matter, since both the low-lying 5*p* states and the high-lying 6*p* states influence the valence bands. For CeN, the 5*p* states were treated as valence states, while the 6*p* states were left out of the calculation, whereas for CeP and CeAs the 5*p* states were treated as core states, and the 6*p*'s like downfolded[37] valence states. In this way,

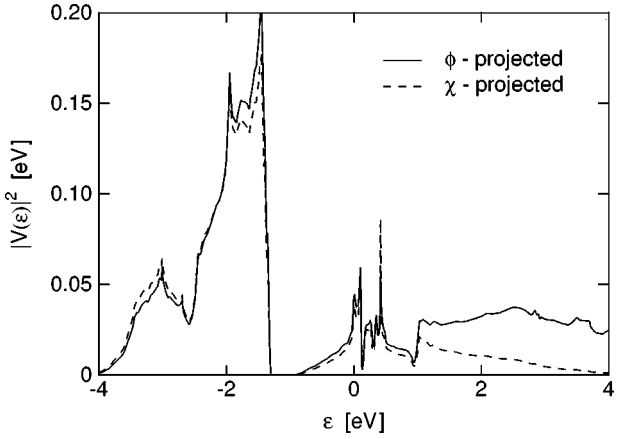

FIG. 1. Effective hybridization functions for CeP calculated from the ϕ_{4f}- and χ_{4f}- projected DOS. The Fermi level is at zero energy.

we were able to converge the calculations in all cases. Probably, the precise treatment of the Ce *p* states does not matter too much for the hybridization function in the low-energy region, as long as the charge distribution of the 5*p* orbital (which surrounds the 4*f* electrons), is reasonably accurate. We used the scalar relativistic approximation, and inserted empty spheres to reduce the errors arising from the ASA. In all spheres other than Ce, the wave function was expanded up to $l=2$. Brillouin-zone summations were done by the tetrahedron method using a mesh of 16^3 **k** points in the full zone, corresponding to 145 irreducible points.

Having performed the band-structure calculation, we need to extract a 4*f*-projected DOS in order to get the starting hybridization function as described in the previous section [Eq. (19)]. This raises the question of which orbital to project down upon. The LMTO ϕ_{4f} functions have the advantage of constituting an orthonormal basis set, but are not continuous, being defined only in a single atomic sphere. The LMTO χ functions, on the other hand, are continuous and differentiable, but if an orthogonal representation is chosen, they will not be very well localized around a particular site. Since it is essential to work with localized orbitals in theories that only include local Coulomb interaction terms, we have chosen to use the so-called tight-binding representation,[37] in which highly localized, but nonorthonormal, orbitals are constructed. To check whether the ambiguity in the choice of *f* orbital is of consequence for our parametrization procedure, we have calculated the effective hybridization function arising from both ϕ and χ projection. In Fig. 1 we show the results for CeP. We note that the results are very similar below the Fermi level, which is the most important region with respect to the many-body calculation. Only at higher energies do the two approaches start to give markedly different results. This indicates that the separation of the electrons in a set of 4*f* states and a surrounding medium is a well-defined concept, also in a first-principles band calculation, and that it is not too important which set of 4*f* states we use. With this result, there is hope that a more complete calculation can be done, using the LMTO Hamiltonian matrix directly instead of the tight-binding matrix. In this work, we have chosen to use the hybridization functions calculated from the ϕ-projected DOS to parametrize the tight-binding Hamiltonian.

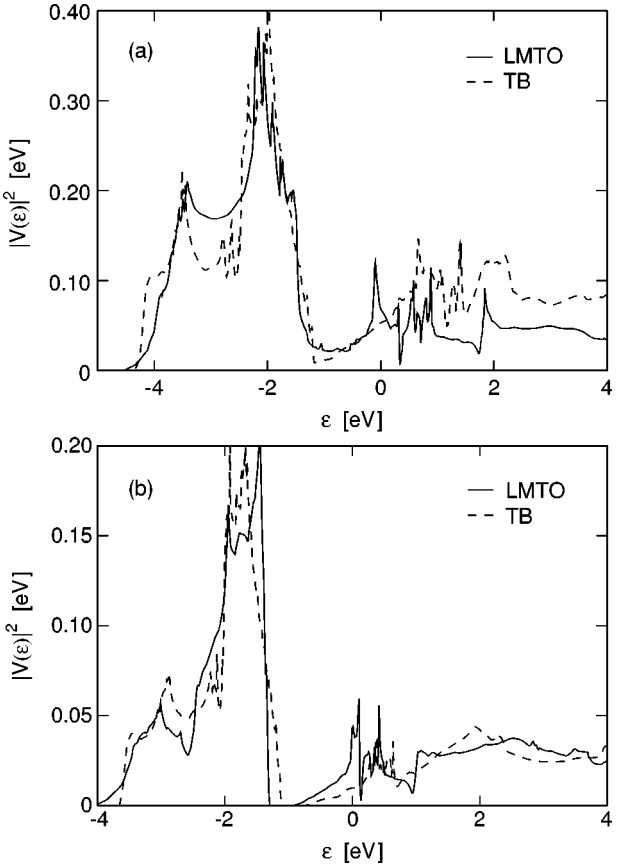

FIG. 2. LMTO and tight-binding hybridization functions for CeN (a) and CeP (b). The Fermi level is at zero energy.

As described in the previous sections, we have parametrized the tight-binding Hamiltonian by first fixing the relative positions of the orbital energies to the values obtained from the LMTO band-center parameters, and afterwards adjusting the various hybridization parameters to match the LMTO hybridization function. All hybridization terms have been included, except for the f-f terms. Only the Slater-Koster σ integrals were taken to be different from zero. In Fig. 2 we compare the tight-binding hybridization functions to the LMTO results. While we have not attempted a perfect fit, it is evident that all the low-energy features of the LMTO hybridization functions are well described by the tight-binding model. The basic trend with increasing atomic number of the ligand, is a reduction of the hybridization strengths, leading to smaller hybridization functions. The most dramatic change occurs from CeN to CeP, where the hybridization function is reduced by more than a factor of 2. From CeP to CeAs a further reduction of ~30% takes place.

2. Atomic calculations

To determine values for the local Coulomb repulsion *U* and the separation between the bare Ce *f* and *d* levels we have performed atomic calculations within the framework of density-functional theory. As in the band calculations, we have worked in the scalar relativistic approximation so that all states with a given orbital angular momentum and number of nodes in the radial function are degenerate. Since Ce gives

off some electronic charge to the ligands in the pnictides, we have done the calculations for free Ce ions of unit positive charge. We model the atom by a Hamiltonian of the form

$$\hat{H}_{at}=\varepsilon_f\hat{n}_f+\varepsilon_d\hat{n}_d+\varepsilon_s\hat{n}_s+\frac{U_f}{2}\sum_{\nu\nu'}\hat{n}_f^{\nu}\hat{n}_f^{\nu'}+U_{df}\hat{n}_f\hat{n}_d+\frac{U_d}{2}\sum_{\nu\nu'}\hat{n}_d^{\nu}\hat{n}_d^{\nu'}, \tag{22}$$

that is, we neglect correlations between the 6*s* states and the rest of the orbitals. The various parameters can now be extracted from a finite number of atomic calculations. Explicitly, we have the equations

$$E[4f^05d^26s^1]-E[4f^15d^16s^1]=\varepsilon_d-\varepsilon_f+U_d-U_{df}, \tag{23}$$

$$E[4f^05d^36s^0]-E[4f^15d^26s^0]=\varepsilon_d-\varepsilon_f+2(U_d-U_{df}), \tag{24}$$

$$E[4f^15d^26s^0]-E[4f^15d^16s^1]=\varepsilon_d-\varepsilon_s+U_d+U_{df}, \tag{25}$$

$$E[4f^15d^16s^1]-E[4f^15d^06s^2]=\varepsilon_d-\varepsilon_s+U_{df}, \tag{26}$$

$$E[4f^15d^26s^0]-E[4f^25d^16s^0]=\varepsilon_d-\varepsilon_s+U_d-U_f. \tag{27}$$

From these equations the parameters $\varepsilon_d-\varepsilon_f, U_f, U_d, U_{df}$ can be determined in terms of the atomic energies. Doing the atomic calculations within the LSDA, we obtain the results $\varepsilon_d-\varepsilon_f=6.03$ eV, $U_f=6.3$ eV, $U_{df}=1.23$ eV, $U_d=0.51$ eV. This confirms that the onsite correlation terms U_{df} and U_{dd}, which are neglected in our band Hamiltonian, are indeed much smaller than the *f*-*f* repulsion. They are, however, large enough that they should be incorporated in a mean-field approximation, since the physics of the Anderson impurity model depends strongly on the position of the *f* level relative to the Fermi level of the medium. A direct incorporation into our tight-binding model is dangerous, since the limited basis set means that the occupation numbers arising in the model are not necessarily representative of the real system. Indeed, our LMTO band-structure calculations show that both the *s* and *p* states of Ce carry some amount of charge (in total about 0.8*e*), while we neglect these degrees of freedom in our band Hamiltonian. Instead, we estimate the Hartree energies from the LMTO occupation numbers. In the many-body calculations, the occupation of the *f* multiplet comes out slightly below 1 for CeP and CeAs, and around 0.8 for CeN. In the LMTO calculations, the *f* occupation comes out to approximately 1.20 for CeN and 1 for CeP and CeAs. We may thus assume that the onset of the correlations will not lead to any significant charge redistributions relative to the LMTO calculations for CeP and CeAs, while for CeN, ~ 0.4 extra electrons will need to be accomodated (primarily) in the Ce-*d* orbitals, since these dominate the DOS near the Fermi level. Therefore, we estimate $\varepsilon_d-\varepsilon_f$ for CeP and CeAs by comparing atomic total energies in the configurations $4f^15d^{1.4}6s^{0.3}6p^{0.48}$ and $4f^05d^{2.4}6s^{0.3}6p^{0.48}$ corresponding to the (ϕ-projected) occupation numbers arising from our LMTO calculations. In this way, we obtain a value for $\varepsilon_d-\varepsilon_f$ of 5.16 eV in a pure LSDA calculation, and 5.62 eV treating the 4*f* state by the SIC-LSDA method. For CeN, it is more difficult to get an accurate estimate, because the *f*-occupation changes considerably as the correlations are turned on. The LMTO calculation yields a Ce-*d* occupation of about 1.6 electrons, and a Ce-*s* occupancy similar to CeP, CeAs. If we assume that $\sim\frac{3}{4}$ of the *f* electrons that are transferred to band states when self-energy effects are included go into the Ce-*d* states (this appears reasonable from the orbital projected DOS), we are led to consider the Ce atomic configurations $4f^15d^{1.9}6s^{0.3}6p^{0.48}$ and $4f^05d^{2.9}6s^{0.3}6p^{0.48}$ (assuming that the 6*sp* occuaptions are as in CeP, CeAs). With this configuration, $\varepsilon_d-\varepsilon_f=4.62$ eV is obtained by treating the Ce 4*f* states within the LSDA approximation, while SIC-LSDA yields $\varepsilon_d-\varepsilon_f=5.07$ eV. Given the values of U_{df} and U_{dd} discussed above, the uncertainties in occupation numbers should not lead to inaccuracies greater than 0.1–0.2 eV in $\varepsilon_d-\varepsilon_f$.

B. Details of the many-body calculations

The impurity calculations to be described in the following were all done on a dense linear mesh, with a spacing of 1 meV on the energy axis, which is much denser than the resolution obtained in present-day photoelectron spectroscopies. The temperature parameter was mostly set at 11.6 K, so that k_BT was equal to the width of the mesh intervals. We have found that this is sufficient to give an accurate numerical calculation, while numerical instabilities start to develop if the temperature is lowered further relative to the energy grid spacing. The mesh extends from -20 to 20 eV in order to get good accuracy in the convolutions.

For impurity model parameters that lead to strong mixing of the f^0 and f^1 configurations it turns out that our self-energy functional does not always yield a positive lattice spectral function. This is a clear sign that the hybridization expansion is inadequate in strongly hybridizing cases. We have treated this problem in the simplest possible manner, by resetting the imaginary part of the self-energy to an infinitesimal value of the correct sign whenever the problem arises. This does not appear to disturb the iterations towards self-consistency, and in the final self-consistent solutions presented in the following the problem is only present in the case of CeN. Even in this rather strongly hybridized case ($n_f\sim 0.8$), the self-energy only has to be reset in an interval of length ~ 0.07 eV in total, and the integral of the reset quantity is $\sim 10^{-3}$ eV^2. For the CeP and CeAs solutions, the spectral function is always positive. Although the existence of this problem is disturbing from a fundamental point of view, we do not consider it to be a problem in practical calculations as long as it only occurs in regions where the magnitude of the spectral function is not controlled by the imaginary part of the self-energy. Still, if one wants to describe more general situations (i.e., with stronger hybridization effects) within this formalism, a remedy for the problem should be sought.

For the **k**-space integration of the lattice Green's function, which constitutes the major computational effort, the Green's function was represented on an energy mesh with variable spacing: In a narrow region around the Fermi level, the spacing was 1 meV, as in the impurity calculation, while in the rest of the energy range the spacing was 10 meV. In this way the sharp structures in the spectrum arising near the

Fermi level are accurately described. The only quantity that needs to be carried over to the impurity calculation is the effective hybridization function, which is fairly smooth away from the Fermi level, and can be interpolated to the denser mesh without problems. The **k**-space integration was done by the Lambin-Vigneron algorithm.[38,19] In this approach, the Green's-function matrix is diagonalized at each frequency point, so that a particular matrix element can be expressed as

$$G_{\mathbf{k}mm'}(\omega)=\sum_n \frac{a^{\mathbf{k}}_{mn} b^{\mathbf{k}}_{nm'}}{\omega-\varepsilon_{n\mathbf{k}}}, \tag{28}$$

with $a^{\mathbf{k}}_{mn}, b^{\mathbf{k}}_{nm}$ being components of the nth left and right eigenvectors of eigenenergy $\varepsilon_{n\mathbf{k}}$. Dividing the irreducible part of the Brillouin-zone into tetrahedra, and expanding the eigenvalues and eigenvectors to linear order within each tetrahedron, one can obtain analytical formulas for the contribution to the Green's function from a single tetrahedron, given eigenvalues and vectors at its corners. We performed the **k**-space integration with a division of 12–16 **k** points along each axis on the coarse energy mesh, and 20–24 **k** points in the high-precision region close to the Fermi level. The large number of **k** points turned out to be necessary for describing the strong p-f mixing arising here accurately.

C. CeP

Of the three Ce monopnictide systems studied here, CeP is the most interesting case, with a very localized Ce 4*f* electron in the ground state, yet showing strong hybridization effects in the low-energy excitations.[6,23,26] Experimentally, CeP is a semimetal with a carrier concentration of 0.3% per formula unit.[20] It has recently been shown that this picture can be reproduced by band-structure calculations within the SIC-LSD approximation.[21] In these calculations, one Ce 4*f* electron is treated as localized (i.e., self-interaction corrected), and does not contribute to the DOS at the Fermi level, but forms a δ-function-like peak at high binding energy (around 7.5 eV). The net result is that a semimetallic gap opens up, the carriers being provided by small electron/hole pockets at the M/Γ points in the Brillouin zone, respectively. This result indicates, that the experimental picture of CeP is that of a 4*f* level very close to integral occupancy, with a correspondingly small contribution to the DOS at the Fermi level. This is in accord with results from photoemission spectroscopy, which show a two-peak structure of the occupied 4*f* DOS, with one peak situated close to (but clearly below) the Fermi level, and another around the bottom of the non-*f* valence bands.[26,6] These are naturally interpreted as deriving from spin (upper peak) and charge excitations (lower peak). In a recent, angle-resolved, photoemission experiment with high resolution, Kumigashira *et al.* determined the position of the upper peak to be about 0.3 eV below the Fermi level, while the lower peak was found to lie around -3 eV.[6] The upper peak appears quite narrow, and shows a small dispersion of $\sim$40 meV (roughly the same as the experimental resolution). The lower peak also displays dispersion effects in position and magnitude, but whether this is due to the actual DOS or to finite-lifetime effects is not clear. It should be noted, that the integrated intensity of the upper peak is at least as high as that of the low one,

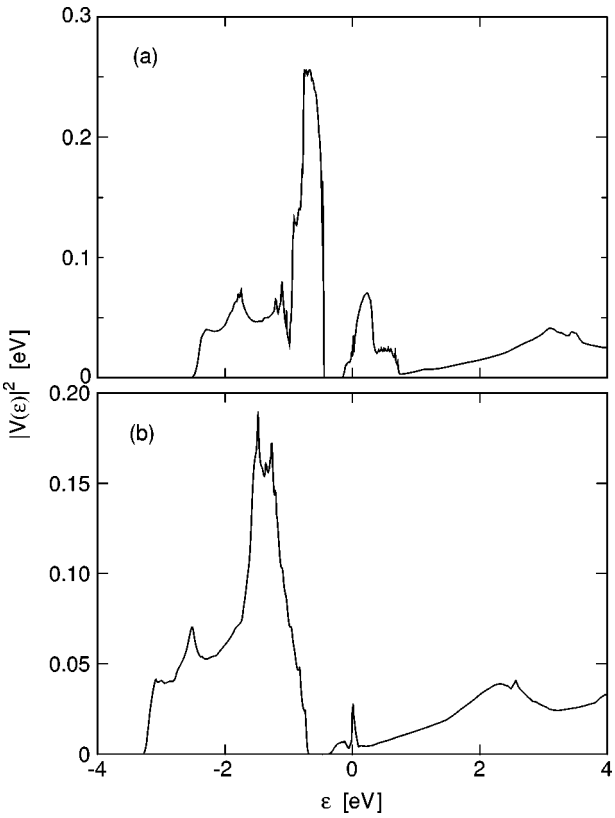

FIG. 3. Effective hybridization functions for CeP in the initial iteration (a), and at self-consistency (b). $\varepsilon_d-\varepsilon_f$ is 5.16 eV. The Fermi level is at zero energy.

which shows that there is a strong effect of the *f*-valence hybridization (in the unhybridized limit, only the charge-excitation peak would be present), in spite of the near-integral *f* occupation. This makes CeP (and to a lesser extent CeAs) a particularly interesting case for study.

In Figs. 2 and 3 the hybridization functions entering various stages of the calculations are shown. Figure 2(b) depicts the LMTO and tight-binding hybridization functions of CeP, to give an idea of the accuracy of our mapping procedure. While the overall fit is quite good, it can be seen that the tight-binding Hamiltonian cannot provide a perfect match to the LMTO results. We have emphasized an accurate description of the hybridization strength below the Fermi level, since this is most important in the many-body calculations. In particular, we have fixed the integrated weight below E_F in the tight-binding model to equal the result of the LMTO calculation. It is seen that the large contribution to the hybridization arising from the occupied P-*p* states is quite well matched, while the description of the *f* resonance near the Fermi level is less accurate. This is probably not too important, since this energy region will lie above E_F in the self-consistent solution. At the present level of approximation, it is probably not worthwhile to pursue a more detailed agreement between these functions.

Figure 3(a) shows the hybridization function obtained by diagonalizing the single-particle part of the tight-binding Hamiltonian after the *f* level has been shifted down to make $\varepsilon_d-\varepsilon_f=5.16$ eV, but without inclusion of any self-energy effects. Apart from shifting the energy positions of the various structures, this modification also enhances the hybridiza-

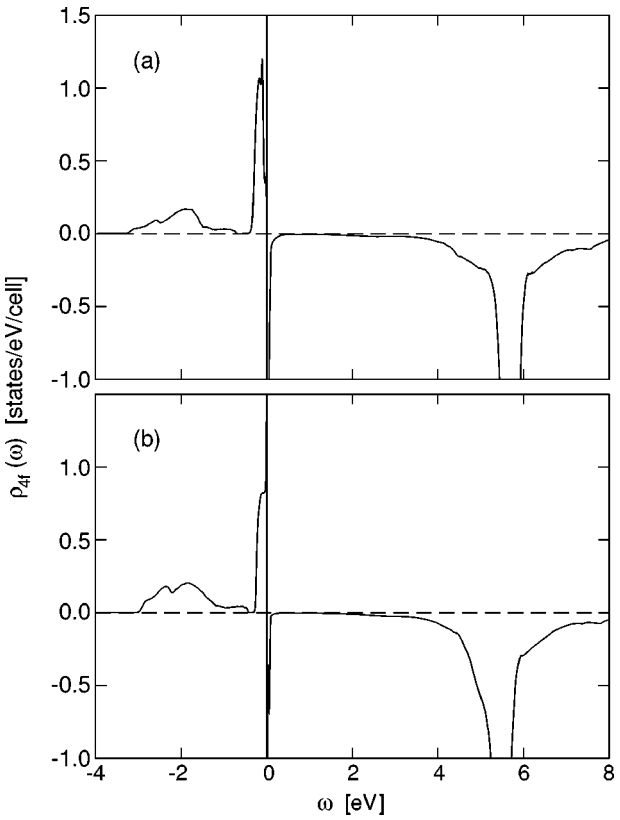

FIG. 4. Ce 4*f*-projected DOS of CeP for $\varepsilon_d-\varepsilon_f$=5.16 eV (a) and $\varepsilon_d-\varepsilon_f$=5.62 eV (b). The spectral weight is plotted positive for occupied states, and negative for unoccupied states.

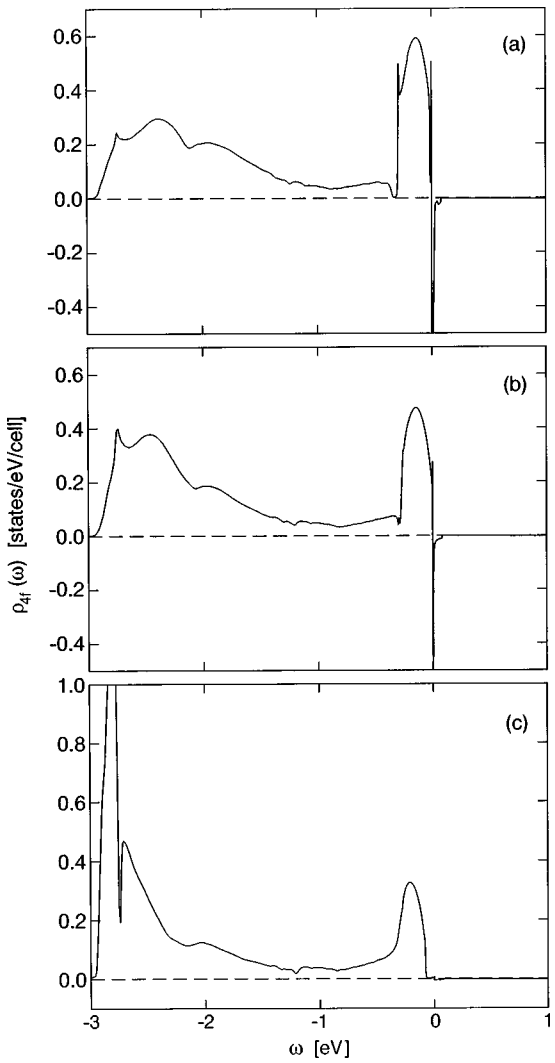

FIG. 5. Same as Fig. 4 for $\varepsilon_d-\varepsilon_f$=6.0 eV (a), 6.2 eV (b), and 6.5 eV (c).

tion between the *f* and *p* states, since they are now rather close in energy. We emphasize that this hybridization function is ''unphysical,'' since it is calculated without taking the *f*-*f* correlation effects into account in any way (not even in a mean-field approximation). When the self-energy effects are turned on, the (''dressed'') *f*-level position is again pulled upwards. Figure 3(b) shows the self-consistent hybridization function, which is seen to be quite close to the initial LMTO result [Fig. 2(b)]. The main difference is that the weight around the Fermi level is strongly affected by the many-body effects in this region, as will be discussed further below.

In Fig. 4(a) the 4*f* DOS arising at self-consistency for the parameters mentioned above (that is, with $\varepsilon_d-\varepsilon_f$ determined by atomic LSDA calculations) is shown. The sign of the spectral function is positive below E_f and negative above. The main features of the DOS are a very narrow peak around the Fermi level, accompanied by a broader structure centered at approximately -0.15 eV, a large f^1-f^2 peak just below 6 eV, and a broad band of states at approximately -2 eV derived from the small *f* components of the occupied *pd* bands. The spectrum is clearly at variance with the experimental picture described above in three respects: First, the DOS at the Fermi level is large, so that this model describes a heavy-fermion state, rather than a semimetal. The 4*f* occupancy comes out as 0.92 electrons. Second, the charge-excitation satellite, which is well defined in the experimental spectrum, is absent here. And third, the peak just below the Fermi level appears too high in energy.

The (weak) delocalization of the 4*f* electron can have two causes: Either the hybridization strength is too large, or the position of the *f* level is too high. At self-consistency, the *f* level position in this calculation is -0.80 eV relative to the Fermi level. The absence of a well-defined charge-fluctuation peak indicates that the latter explanation is the appropriate one (a weaker hybridization would not enhance the weight at the lower band edge). In Fig. 4(b) we therefore show the spectral function arising from a calculation in which the $\varepsilon_d-\varepsilon_f$ separation was taken to be 5.62 eV as obtained in a SIC-LSDA atomic calculation. There is now more weight in the states at higher binding energy, and the *f* occupancy has increased to about 0.96. However, the DOS at the Fermi level is still high, so this calculation does not constitute a satisfactory description of the experimental situation either. The self-consistent position of the *f* level relative to E_f is now -1.05 eV. That our initial downshift of the *f* level by 0.46 eV results in a final shift of only 0.25 eV has a simple explanation: When the *f*-level position is moved down, more electrons are transferred to the *f* state from the other orbitals, which means that the Fermi-level position relative to ε_p and ε_d goes down, counteracting the downward shift of the *f* level.

To investigate whether the model is capable of describing the experimental situation at all, we continue to lower the

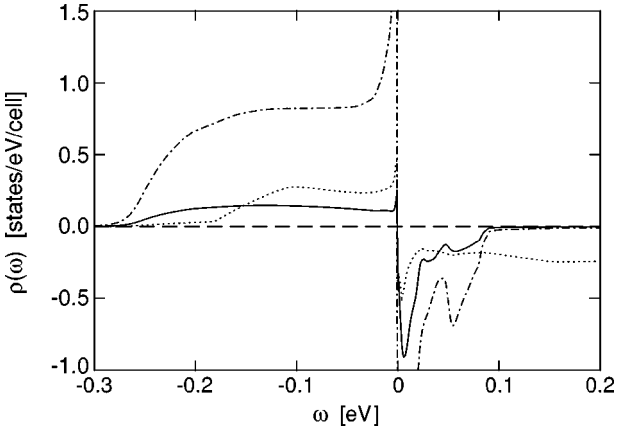

FIG. 6. Orbital projected DOS of CeP close to the Fermi level. The solid line is P-*p* states, the dashed line is Ce *d*, and the dash-dotted line is Ce *f*. Sign convention as in Fig. 4.

f-level position. In Fig. 5 we show spectral functions for $\varepsilon_d - \varepsilon_f$ values of 6.0, 6.2, and 6.5 eV. We notice that the charge-excitation peak rises sharply as the $\varepsilon_d - \varepsilon_f$ value becomes larger than 6 eV. At the same time, the *f*-level occupancy becomes close to 1, so that the position of the self-consistent *f* level now follows the $\varepsilon_d - \varepsilon_f$ value without the counteracting effect mentioned above. It appears that an $\varepsilon_d - \varepsilon_f$ value of approximately 6.2–6.3 eV would give a good description of the experimental spectrum (at least as good as we can expect from the present model). The sensitivity of the spectral function to small changes of the *f*-level position in this parameter region means that one will probably need a more accurate model than the present one to do reliable *ab initio* calculations for this compound. Still, our results show that the parameters obtained by LSDA and SIC-LSDA calculations are of the correct magnitude, and at least constitute a good starting point for seeking refinements of the theory.

In Fig. 6 we show the *p*, *d*, and *f* DOS close to E_F for the calculation with $\varepsilon_d - \varepsilon_f = 5.62$ eV. It is clear that the *p* and *d* DOS are significantly perturbed by hybridization to the *f*-electron heavy-fermion states. However, the modification is not very strong, and is only seen clearly because the ''bare'' *pd* DOS shows a semimetallic gap in this region.

It is interesting to follow the evolution of the hybridization function in the vicinity of the Fermi level as the *f* level is shifted downwards. This is shown in Fig. 7, together with the 4*f* spectral function. The hybridization strength is seen to evolve more or less with the spectral density. In particular, the weight at the Fermi level decreases as the position of ε_f is lowered. In a region with a large 4*f* self-energy, the asymptotic form of Eq. (19) is

$$|V(\varepsilon)|^2 = \frac{1}{\pi} \operatorname{Im} \sum_{\mathbf{k}} \sum_{\lambda} \frac{|V^{\mathbf{k}}_{\lambda\nu}|^2}{\varepsilon - \varepsilon_\lambda - i0^+}. \tag{29}$$

Here λ enumerates eigenstates of the *pd* system without inclusion of the coupling $V^{\mathbf{k}}_{\lambda\nu}$ to the *f* states (indexed by ν). As all *f* states are equivalent in our model, the expression (29) is independent on ν. Since the *f* states do not influence the energy spectrum of the λ states at all, it is clear that this function will not show the *f*-related peak structures at the Fermi level. In Figs. 7(a)–7(c) the intensity of the structure

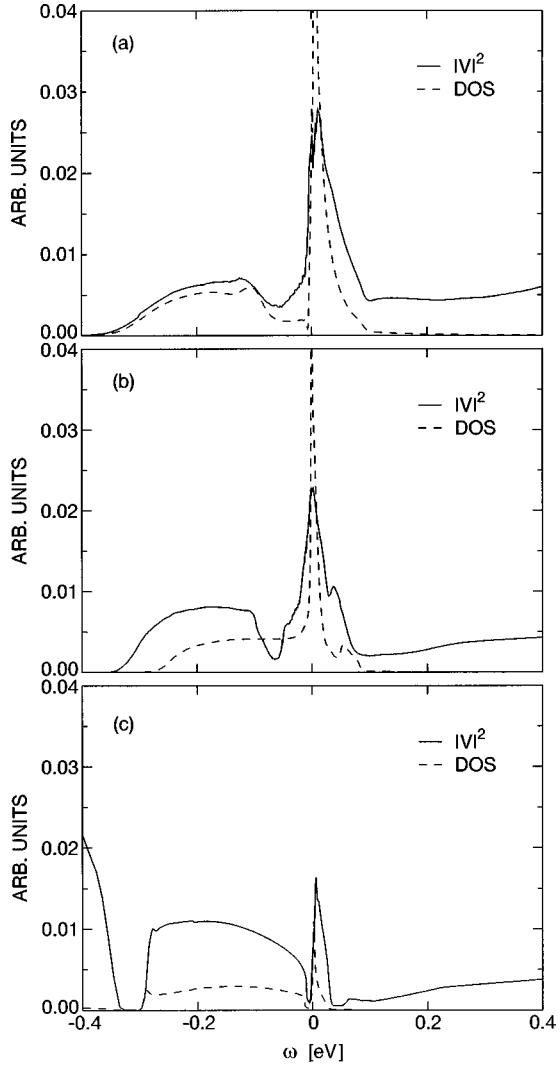

FIG. 7. Hybridization function near E_F for different *f*-level positions: (a) $\varepsilon_d - \varepsilon_f = 5.16$ eV, $n_f = 0.92$; (b) $\varepsilon_d - \varepsilon_f = 5.62$ eV, $n_f = 0.96$; (c) $\varepsilon_d - \varepsilon_f = 6.0$ eV, $n_f = 0.995$. The hybridization functions are shown together with the (scaled) 4*f* DOS (dashed lines). In all figures, the Fermi level is at zero energy.

right at the Fermi level is seen to decrease as the *f* electron becomes more and more localized, but the unhybridized limit is quite far from being realized. Note, in particular, the growth of the hybridization strength arising from the many-body states at ~ -0.2 eV.

Kumigashira *et al.*[6] have recently presented evidence for a small dispersion in the *f*-related peak just below the Fermi level in angle-resolved photoemission spectroscopy. To investigate this phenomenon, we have extracted angle-resolved spectral functions from our self-consistent calculations. In Fig. 8 we show an example along the Γ-X direction in the Brillouin zone. The curves were obtained by fixing the (conserved) surface-parallel component of the **k** vector at some point on the Γ-X line, while integrating the perpendicular component across the Brillouin zone. The numbers labeling the different curves gives the distance from Γ in the surface plane in units of $2\pi/a$. The magnitude of the dispersion is ~ 0.05 eV, and the width of the structure is ~ 0.2 eV. Both of these quantities are in reasonable agreement with the experimental results, which find a dispersion of ~ 0.04 eV, and a

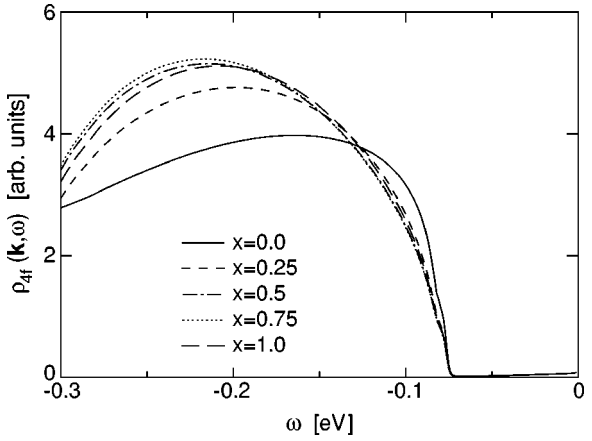

FIG. 8. Ce 4*f*-projected DOS of CeP for states with **k**-vector component in the [100] plane along the Γ-X direction. The length of the Γ-X component is $x(2\pi/a)\varepsilon_d-\varepsilon_f$ is 6.5 eV. The Fermi level is at zero energy.

peak width of ~0.2 eV. The trend that the peak position moves down in energy as one goes from Γ towards X, with a final upturn close to the zone edge, is also (qualitatively) in agreement with the photoemission results. However, the position of the structure, and the precise energy differences between the various **k** points are not predicted correctly. The high position of the peak compared to the experiment could be remedied by a rescaling of the hybridization function, but this also reduces the total weight of the structure considerably. Probably, a more detailed description of the 4*f* multiplet structure (and perhaps a more realistic modeling of the photoemission experiment) would be needed to reproduce the results in greater detail. Conceptually, however, it is an important realization, that dispersion effects can appear in a model of the kind discussed here, even in the present case of rather strongly localized *f* electrons.

D. CeAs

The physical properties of CeAs are quite similar to those of CeP, except that the hybridization of the Ce 4*f* orbitals to the surroundings is weaker. This is clearly seen in photoemission experiments as a reduction of the spin-fluctuation peak close to the Fermi level, and is also borne out by our LMTO calculations. Total-energy studies with the SIC-LSDA formalism have indicated that the structural properties of the Ce monopnictides may be understood as caused by a decrease of the 4*f* hybridization with increasing ligand atomic number.[21] Like CeP, CeAs is also semimetallic, with a carrier concentration of 0.24%.[39]

In Fig. 9 the 4*f* DOS is shown as calculated within our model for three different values of $\varepsilon_d-\varepsilon_f$ (5.16 eV, 5.62 eV, and 6.0 eV). The major trends are the same as for CeP: The weight in the upper part of the occupied spectrum is reduced as the *f* level moves down, and a clear charge-excitation peak develops at the lower band edge. Again it is observed, that the *ab initio* positions of the *f* level are too high to give a good agreement with the experimental facts. Both the LSDA and SIC-LSDA values for $\varepsilon_d-\varepsilon_f$ give a metallic, heavy-fermion-like system. The self-consistent *f*-level occupancies are 0.94, 0.98, and 0.997, respectively. The positions of the *f* level relative to E_F at self-consistency

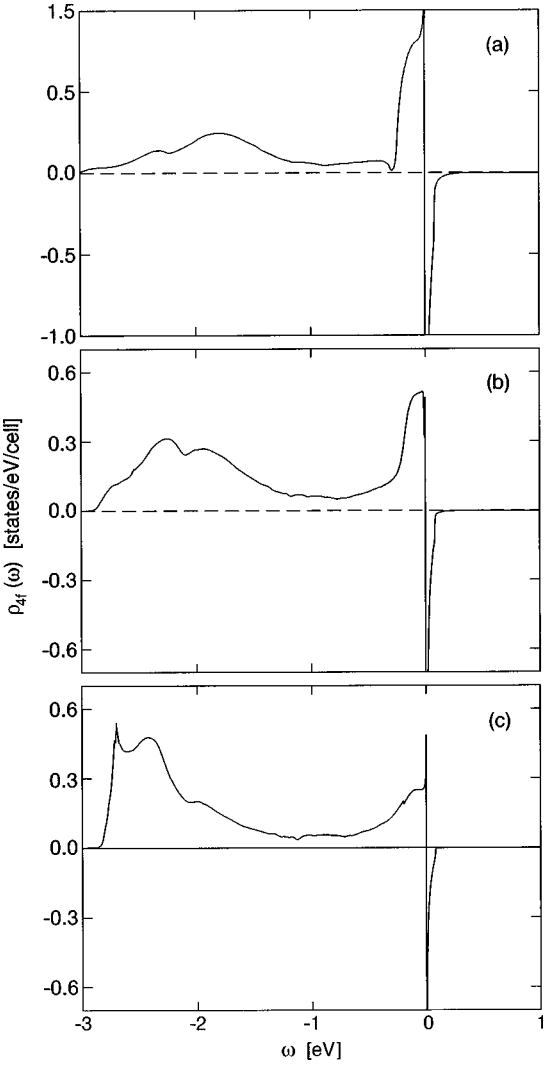

FIG. 9. Ce 4*f*-projected DOS of CeAs for $\varepsilon_d-\varepsilon_f$=5.16 eV (a), $\varepsilon_d-\varepsilon_f$=5.62 eV (b), and $\varepsilon_d-\varepsilon_f$=6.0 eV (c). Sign convention as in Fig. 4.

are −0.97 eV, −1.31 eV, and −1.62 eV, respectively, for the three different choices of $\varepsilon_d-\varepsilon_f$. Comparing the positions and the relative weight of the *f*-related peaks to experiments,[23,26] the calculation with $\varepsilon_d-\varepsilon_f$=6.0 eV gives a spectral function closest to the experimental one. In the limit of extremely weak hybridization, the 4*f* DOS would consist of a single peak around the bare *f*-level position. The calculated spectra of Fig. 9 do not show a peak at this energy, so it can be concluded that hybridization effects still play a decisive role in determining the structure of the excitation spectrum.

Compared to the CeP spectrum, the CeAs DOS has less weight in the spin-fluctuation peak, and more in the states at higher binding energies. This is consistent with experimental findings,[26,23] which gives the ratio between the upper and lower peak as 2:1 and 1:1 for CeP and CeAs, respectively. These ratios are extracted from difference spectra, and it is not clear how they should be calculated from our DOS, since a substantial part of the 4*f* weight in our calculations lie in the region of the P,As *p* bands, and since our calculations do not include matrix element effects. Qualitatively, however, this trend seems well explained by the model. The position

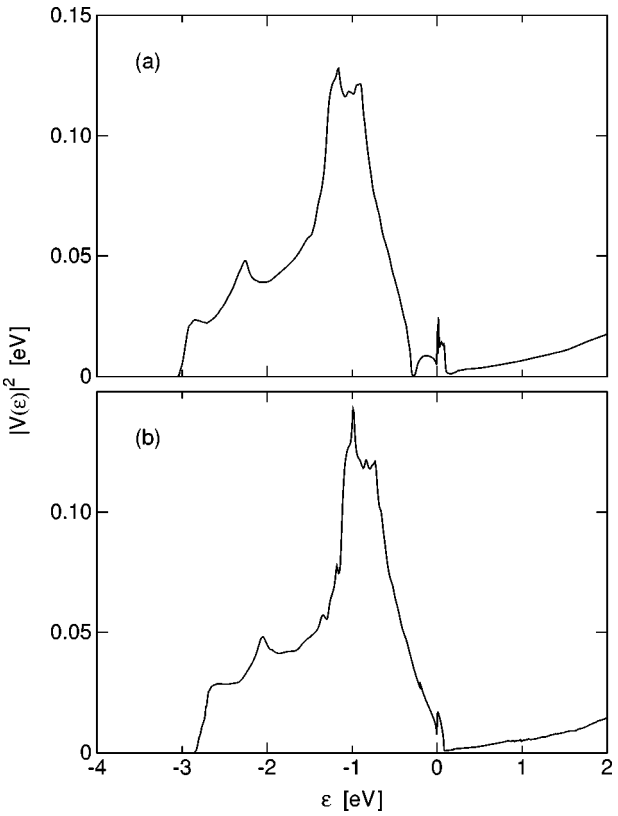

FIG. 10. Effective hybridization function of CeAs at self-consistency for $\varepsilon_d-\varepsilon_f=5.16$ eV (a), and 6.0 eV (b). The Fermi level is at zero energy.

of the upper peak found in these experiments is ~ 0.6 eV below the Fermi energy for both CeP and CeAs, which is clearly at variance with our results, but also with the more recent angle-resolved data for CeP.[6] Assuming that the correct position is 0.3–0.4 eV below E_F, as in CeP, our peak still appears too high, but the difference is of the order of 0.1 eV and could be modified in a more complete treatment. The broadening of the peak in CeAs relative to CeP is connected to the position of the *p* band relative to the Fermi level: In CeP there is a gap in the hybridization function just below the structure related to the many-body states, whereas in CeAs the edge of the *p* states moves very close to the Fermi level (Fig. 10). This result is not supported by the photoemission experiments quoted, but the widths found experimentally are, in any case, larger than the calculated widths, and may in part be caused by the finite experimental resolution. For CeP, the more recent high-resolution measurements indeed find a smaller width of the spin-fluctuation structure.

In Fig. 10 the hybridization function at self-consistency is shown for two different positions of the *f* level. In comparison to the CeP case, the strucure near the Fermi level is now less pronounced, and closer to the asymptotic case of unhybridized *pd* bands.

E. CeN

CeN is the only material in the Ce monopnicitide series showing a metallic ground state. The *f* electron delocalizes, due to a stronger *pd-f* hybridization, and a narrow peak in the DOS develops around the Fermi level. In addition to this peak, photoemission experiments reveal a shoulder structure at ~ -0.3 eV and a second peak at -1.2 eV, both of which are thought to be *f* related.[22,23] At higher binding energies a valence band extending down to about -4 eV is observed, but in contrast to CeP and CeAs, no clear sign of an *f*-state charge excitation peak at the lower valence-band edge is observed. This indicates that the *f* weight in this region resides in bandlike states.

Schneider *et al.*[25] analyzed a variety of spectroscopic results using the Gunnarsson-Schönhammer approach,[4] and found that an *f*-level position of -0.8 eV relative to E_F and a hybridization strength leading to an *f* occupation of 0.8 electrons gave good fits to the experimental spectra. The analysis of Schneider *et al.* was done with a *U* value of 7 eV and an *f*-level degeneracy of 6 (neglecting the $j=\frac{7}{2}$ states), so their many-body calculation is quite similar to the one implemented here, except for the more realistic description of the hybridization function in the present work. Patthey *et al.*[24] did a first-order perturbation calculation including spin-orbit splitting, and found agreement with photoemission spectra with an *f*-level position of -1.0 eV and a $j=\frac{5}{2}$ occupation of 0.86. These authors interpreted the shoulder structure at -0.3 eV as caused by a $j=\frac{5}{2}\rightarrow j=\frac{7}{2}$ transition, and the peak at -1.2 eV as being caused by emission from localized f^1 levels, stabilized by proximity to the surface or vacancy defects. The last interpretation is indirectly supported by our calculations, since we do not find any sign of a bulk state at this energy.

Due to the strong hybridization, CeN is the most difficult of the monopnictides to describe within our tight-binding model. The LMTO calculation for this compound yields a separation of 3.7 eV between the Ce *d* and *f* band centers, but to obtain a reasonable match of the hybridization functions, we have found it necessary to reduce the separation of the tight-binding levels to 2.7 eV. This is an indication that the small basis set is no longer adequate to mimic the full LMTO calculation. The LMTO and initial TB hybridization functions are shown in Fig. 2(a). The LMTO hybridization function was, as in the other compounds, calculated from the ϕ_{4f}-projected DOS. In CeN, unlike the other compounds studied here, the integrated weight of the hybridization function below the Fermi level is somewhat different ($\sim 20\%$) in the ϕ- and χ-projected calculations, so in this case the ambiguity in the definition of the 4*f* orbitals is not completely without consequence.

As it turns out, it is impossible to describe the experimental situation even approximately by the parameters obtained from *ab initio* calculations. The strong hybridization puts a large weight on the f^0 impurity configuration, while the f^2 weight remains low due to the large value of *U*. As a result, very low *f* occupancies (of approximately 0.3 electrons) are predicted. Therefore, it is clear, that an *ab initio* theory of CeN would have to be considerably more sophisticated than the present approach, and our main reason for including this compound in the discussion is to investigate what kind of improvements are likely to be necessary.

Since the delocalization of the Ce 4*f* electron is mostly determined by the ratio between the hybridization strength and the *f*-level position relative to the Fermi level, the requirement of $n_f=0.8$ can be met by a range of parameters if we allow for adjustment of both quantities. If we additionally

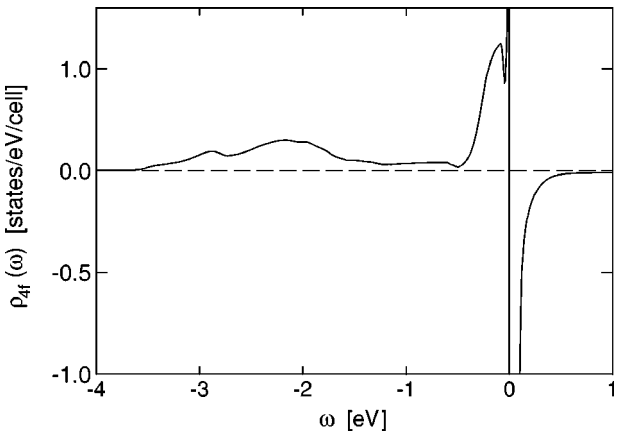

FIG. 11. Correlated 4*f*-projected DOS for CeN. Sign convention as in Fig. 4.

require that no clear *f*-electron peak should develop at the lower band edge we do at least obtain a lower bound on ε_f. It is not our intention here to make a detailed fit of parameters to experimental information, but only to investigate the behavior of the model as we go towards the regime of mixed valence. In Fig. 11 we show a Ce 4*f* spectrum calculated with parameters chosen to mimic the above-mentioned results of spectroscopic fits. Thus, n_f is equal to 0.82, and the position of the *f* level relative to E_F is -1.02 eV. This is obtained by rescaling the hybridization strength with a factor close to two, and putting $\varepsilon_d-\varepsilon_f=5.55$ eV. This value of $\varepsilon_d-\varepsilon_f$ is ~ 0.5 eV lower than the values required to match the experimental spectra of CeP, CeAs, similar to the difference in the values from the atomic calculations. It is thus a consistent trend in all three compounds, that the *ab initio* estimate of the *f*-level position is too high to reproduce the experimental spectra. A possible explanation for this could be that we are using the same hybridization function to describe both the f^0-f^1 and f^1-f^2 couplings in the impurity model. Gunnarson and Jepsen[40] have argued that the hybridization function to be used for the f^1-f^2 matrix elements should be calculated with a doubly occupied 4*f* wave function, which would be considerably expanded compared with the singly occupied function used for the f^0-f^1 hybridization. As a result, the f^1-f^2 coupling strength could be several times larger than the f^0-f^1 coupling. The leading effect of this modification would be to favor occupation of the f^1 configuration, since the ''effective'' f^1-level position is shifted downwards by the coupling to f^2 states. We have not investigated the effect in this work, since we at present have no parameter-free scheme for estimating the enhancement of the f^1-f^2 coupling, but it is a problem that should be addressed in a more complete treatment of Ce compounds. A similar effect would arise from the inclusion of the full *f* multiplet ($N_f=14$), but this would also increase the f^0-f^1 coupling, so the combined result of this modification is less clear.

The necessary rescaling of the hybridization strength, on the other hand, appears surprisingly large, in light of the fact that no significant rescaling was needed for the other compounds. A possible explanation could be the differences in occupation numbers. For CeP and CeAs we had approximate consistency between the *f*-occupation numbers of the LMTO and many-body calculations. In the case of CeN, the occupation of the LMTO 4*f* orbital is about 1.2, while the many-body occupation is only 0.8 electrons. This difference in occupation numbers would make the *f* orbital too large in the LMTO calculation, increasing the hybridization to the other orbitals. Whether this explanation is correct can only be checked by performing calculations in which the many-body–related changes in occupation numbers are incorporated in the band calculation in a self-consistent manner.

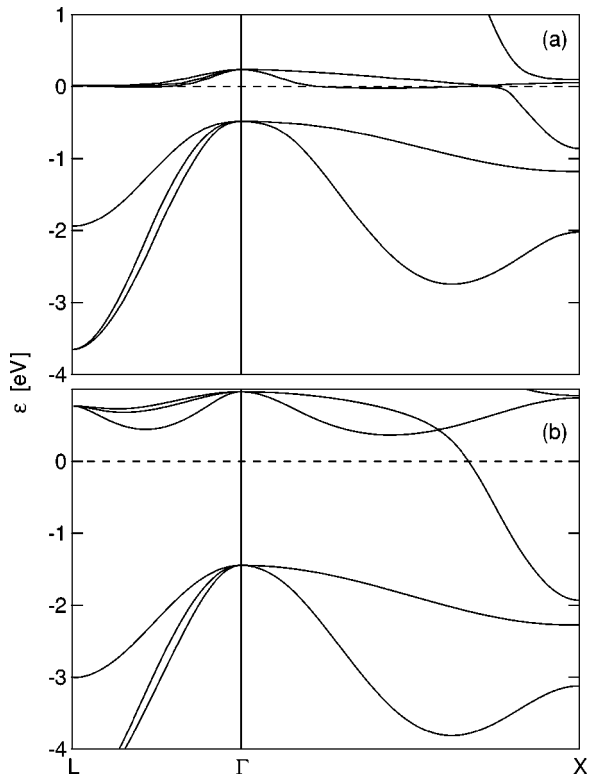

FIG. 12. (a) Valence-band structure of CeN with self-energy effects included. The curves were obtained by finding, at each **k** point, the energies ω, where Real$(\omega-\varepsilon_{n\mathbf{k}})=0$, $\varepsilon_{n\mathbf{k}}$ being the *n*th eigenvalue of the Green's-function matrix at the point **k**. The dashed line indicates the Fermi level. (b) Tight-binding bands without inclusion of self-energy effects, as obtained with parameters matched to the LMTO calculation.

The most prominent features of the 4*f* spectrum shown in Fig. 11 are the very narrow band arising around E_F and the shoulder structure appearing just below, at ~ -0.15 eV. The width of the narrow band is only about 0.1 eV, which is much smaller than the results usually obtained in band theory. The energy derivative of the self-energy at the Fermi level (which is a measure of the quasiparticle mass enhancement) is ~ 5 in this calculation. Still, the **k**-resolved spectra show strong quasiparticle peaks in this region, so that a dispersion relation of ε vs **k** can be extracted. Thus, the model in this case describes a heavy-fermion-like state, featuring fermi-liquid-like excitations with strong correlation-induced mass enhancements.

In Fig. 12 plots of the band structure along the Γ-X and Γ-L directions in **k** space are shown. Figure 12(a) shows the quasiparticle bands with self-energy effects included, while Fig. 12(b) shows the bare tight-binding bands calculated with the parameters matched to the LMTO hybridization function (i.e., with $\varepsilon_d-\varepsilon_f=2.7$ eV). The inclusion of many-body effects clearly leads to the formation of a set of narrow bands

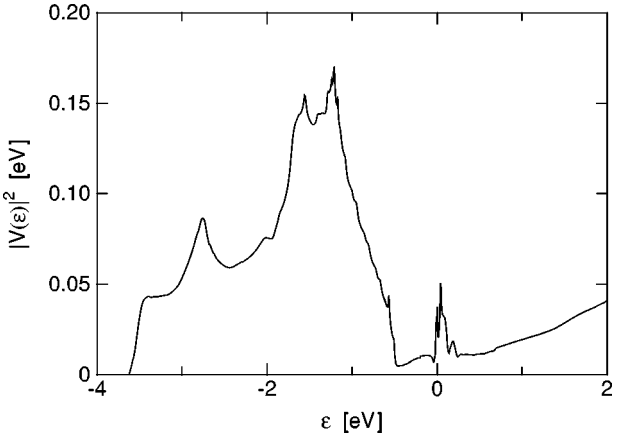

FIG. 13. Self-consistent effective hybridization function for CeN, with parameters as described in the text. The Fermi level is at zero energy.

close to the Fermi level. However, there is still a noticeable dispersion around the Γ point. Comparison of Figs. 12(a) and 12(b) shows that the bands in the vicinity of the Fermi level are significantly narrowed, in accord with the calculated mass enhancement factor ~ 5. The lower-lying bands are largely unaffected by the correlation effects. We emphasize that the ''bands'' in Fig. 12(a) do not constitute the only contribution to the DOS of CeN. The satellite structure appearing just below the HF peak in Fig. 11 arises from the imaginary part of the self energy, i.e., the single-particle states in this energy region have short lifetimes.

In comparison with the experimental photoemission spectra,[22–24] it is interesting to notice, that the present model, which contains no spin-orbit effects, still predicts a shoulder structure at an energy about 0.2 eV below E_F. The same shoulder structure is less pronouncedly found for CeP in Fig. 4 and for CeAs in Fig. 9. The states in this structure are short-lived (i.e., they have a large imaginary self-energy component) and are very weakly dispersing. They arise here because the self-consistent hybridization function (shown in Fig. 13 for CeN) develops a peak at the Fermi level corresponding to the *f* bands appearing here. The satellite structures are created at the back edge of this hybridization peak and are analogous to the charge excitation peaks arising at the lower valence band edge in CeP and CeAs. It is unclear how this structure would be modified in the presence of a spin-orbit split *f* multiplet, but the present result shows that direct extraction of spin-orbit splitting from photoemission experiments may be dangerous.

IV. CONCLUSIONS AND OUTLOOK

In the present work we have described a method for solving strongly correlated lattice problems by means of the dynamical mean-field theory. The method has been applied to a realistic model of the Ce monopnictide systems CeN, CeP, and CeAs. The model has been parametrized using results of *ab initio* atomic and band-structure calculations, and it has been shown that the main physical trends and features of the compounds can be reproduced in this way. Furthermore, we have demonstrated, that a fairly accurate quantitative account of experimental results can be achieved by adjustment of a single parameter (the position of the Ce 4*f* level), in the case of CeP and CeAs, while for CeN a rescaling of the hybridization parameters is also necessary. In particular, we have shown that dispersion effects can occur in the Ce 4*f*-projected DOS, even in cases where the *f* occupation is close to 1. The parameter dependence of the self-consistent effective hybridization function has been investigated, and it has been found to resemble the uncorrelated hybridization rather well, except in energy regions where there is a sizeable density of correlated Ce 4*f* states.

The results presented in this paper raise several questions, but are also promising in at least two respects: Firstly, it is very encouraging, that the model, qualitatively and often quantitatively, is able to account for all features of the experimental spectra of Ce monopnictide compounds. Secondly, it is interesting, that the parameters obtained from *ab initio* calculations come quite close to the ones needed for a detailed match of the experimental picture, and that they (at least for CeP, CeAs) are not very sensitive to the precise way of defining the Ce 4*f* orbital in the LMTO formalism. In light of this, the obvious next step seems to be an incorporation of the many-body calculational scheme presented here directly into an *ab initio* LMTO band structure code, thus providing a more detailed description of the single-particle part of the Hamiltonian, and possibly including spin-orbit effects. A calculation of this kind would be computationally demanding, but not prohibitive.

ACKNOWLEDGMENTS

The authors wish to thank Professor V. I. Anisimov for valuable discussions, stimulating our interest in dynamical mean-field theory. This work has benefited from collaborations within the Human Capital and Mobility Network on ''*Ab initio* (from electronic structure) calculations of complex processes in materials'' (Contract No. ERBCHRXCT930369).

APPENDIX: SOLUTION METHOD FOR THE IMPURITY PROBLEM

In this appendix, the solution of the single-impurity problem will be discussed in greater detail. Most of our discussion will be focused on the calculation of the thermodynamic potential, since this is formally simpler, yet contains all the ingredients needed for the evaluation of the Green's function. For simplicity, we shall consider the case where all impurity states are equivalent.

We follow the approach of Keiter and Morandi[41] and write the partition function as

$$Z=\mathrm{Tr}[e^{-\beta(\hat{H}-\mu)}]=\frac{1}{2\pi i}\oint_C d\omega e^{-\beta(\omega-\mu)}\mathrm{Tr}\left(\frac{1}{\omega-\hat{H}}\right), \tag{A1}$$

by the residue theorem, with the contour C chosen so as to encircle all poles of the resolvent operator. μ is the chemical potential, which in the following will be taken to be equal to zero to simplify the notation. The variable ω is understood to carry an infinitesimal imaginary part. To perform the trace,

we choose a basis consisting of f^0, f^1, and f^2 configurations in combination with conduction electron states N_c as follows:

$$|N_c\rangle = \hat{c}^\dagger_{\nu_1\varepsilon_1}..\hat{c}^\dagger_{\nu_N\varepsilon_N}|\text{vac}\rangle,$$
$$|N_c;\nu\rangle = \hat{c}^\dagger_{\nu_1\varepsilon_1}..\hat{c}^\dagger_{\nu_N\varepsilon_N}\hat{f}^\dagger_\nu|\text{vac}\rangle, \tag{A2}$$
$$|N_c;\nu\nu'\rangle = \hat{c}^\dagger_{\nu_1\varepsilon_1}..\hat{c}^\dagger_{\nu_N\varepsilon_N}\hat{f}^\dagger_\nu\hat{f}^\dagger_{\nu'}|\text{vac}\rangle.$$

We work in the grand canonical ensemble so that the particle number as well as the total energy is variable. This allows us to split the trace into a sum over band states and a sum over the various impurity occupations. Shifting the integral by the energy of the unperturbed conduction electrons, and dividing by their partition function Z_c we obtain

$$Z_f \equiv \frac{Z}{Z_c} = \frac{1}{2\pi i}\oint d\omega \sum_{N_c}\frac{e^{-\beta E_{N_c}}}{Z_c}e^{-\beta\omega}\left[\left\langle N_c\left|\frac{1}{\omega-\hat{H}_{N_c}}\right|N_c\right\rangle + \sum_\nu\left(\left\langle \nu;N_c\left|\frac{1}{\omega-\hat{H}_{N_c}}\right|N_c;\nu\right\rangle + \sum_{\nu'>\nu}\left\langle \nu\nu';N_c\left|\frac{1}{\omega-\hat{H}_{N_c}}\right|N_c;\nu\nu'\right\rangle\right)\right], \tag{A3}$$

$$\hat{H}_{N_c} = \hat{H} - E_{N_c}, \quad E_{N_c} = \sum_{m=1}^{N}\varepsilon_m, \quad Z_c = \sum_{N_c} e^{-\beta E_{N_c}}. \tag{A4}$$

Introducing the ''configurational Green's functions'' (not to be confused with the physical Green's function) as

$$G^{(0)}(\omega) = \sum_{N_c}\frac{e^{-\beta E_{N_c}}}{Z_c}\left\langle N_c\left|\frac{1}{\omega-\hat{H}_{N_c}}\right|N_c\right\rangle,$$
$$G^{(1)}_\nu(\omega) = \sum_{N_c}\frac{e^{-\beta E_{N_c}}}{Z_c}\left\langle \nu;N_c\left|\frac{1}{\omega-\hat{H}_{N_c}}\right|N_c;\nu\right\rangle, \tag{A5}$$
$$G^{(2)}_{\nu\nu'}(\omega) = \sum_{N_c}\frac{e^{-\beta E_{N_c}}}{Z_c}\left\langle \nu\nu';N_c\left|\frac{1}{\omega-\hat{H}_{N_c}}\right|N_c;\nu\nu'\right\rangle,$$

and the corresponding spectral functions,

$$\rho^{(0)}(\omega) = \frac{1}{\pi}\,\text{Im}\,G^{(0)}(\omega), \text{ etc.}, \tag{A6}$$

the partition function can be written as

$$Z_f = \int_{-\infty}^{\infty} d\omega\, e^{-\beta\omega}\left[\rho^{(0)}(\omega) + \sum_\nu\left(\rho^{(1)}_\nu(\omega) + \sum_{\nu'>\nu}\rho^{(2)}_{\nu\nu'}(\omega)\right)\right]. \tag{A7}$$

All we need to describe the thermodynamics of the impurity model is thus to determine the configurational Green's functions. This is done by a series expansion of the resolvent operator. The Hamiltonian is split into a part $\hat{H}^D$ that is diagonal in the chosen basis, and a part $\hat{V}$ that is not, i.e., $\hat{H} = \hat{H}^D + \hat{V}$. Thus

$$\frac{1}{\omega-\hat{H}_{N_c}} = \sum_{n=0}^{\infty}\frac{1}{\omega-\hat{H}^D_{N_c}}\left(\hat{V}\frac{1}{\omega-\hat{H}^D_{N_c}}\right)^n. \tag{A8}$$

To determine the Green's function for some configuration m, we must evaluate

$$G^{(m)}(\omega) = \sum_{N_c}\frac{e^{-\beta E_{N_c}}}{Z_c}\left\langle m;N_c\left|\frac{1}{\omega-\hat{H}_{N_c}}\right|N_c;m\right\rangle = \sum_{N_c}\frac{e^{-\beta E_{N_c}}}{Z_c} \times\left\langle m;N_c\left|\frac{1}{\omega-\hat{H}^D_{N_c}}\sum_{n=0}^{\infty}\left(\hat{V}\frac{1}{\omega-\hat{H}^D_{N_c}}\right)^n\right|N_c;m\right\rangle. \tag{A9}$$

The expectation values of the operator $\hat{H}^D_{N_c}$ are independent of the state of the conduction electrons since their energy has been explicitly subtracted, i.e., we can write

$$\left\langle m;N_c\left|\frac{1}{\omega-\hat{H}^D_{N_c}}\right|N_c;m\right\rangle \equiv G^{(m)}_0(\omega). \tag{A10}$$

Introducing the projection operator

$$\hat{O}^m_{N_c} = 1 - |N_c;m\rangle\langle m;N_c|, \tag{A11}$$

the $G^{(m)}$ can be expressed as

$$G^{(m)}(\omega) = G^{(m)}_0(\omega)\sum_{n=0}^{\infty}\left[G^{(m)}_0(\omega)\sum_{N_c}\frac{e^{-\beta E_{N_c}}}{Z_c} \times\left\langle m;N_c\left|\sum_{n'=0}^{\infty}\left(\hat{V}\hat{O}^m_{N_c}\frac{1}{\omega-\hat{H}^D_{N_c}}\right)^{n'}\hat{V}\right|N_c;m\right\rangle\right]^n \equiv \frac{1}{(G^{(m)}_0(\omega))^{-1}-\Sigma^{(m)}(\omega)}, \tag{A12}$$

thus defining the configurational self-energy $\Sigma^{(m)}$,

$$\Sigma^{(m)}(\omega) = \sum_{N_c}\frac{e^{-\beta E_{N_c}}}{Z_c} \times\left\langle m;N_c\left|\sum_{n'=0}^{\infty}\left(\hat{V}\hat{O}^m_{N_c}\frac{1}{\omega-\hat{H}^D_{N_c}}\right)^{n'}\hat{V}\right|N_c;m\right\rangle. \tag{A13}$$

To arrive at a manageable approximation for the self-energies we write out the lowest-order terms of the series (A13) for the different configurations:

$$\Sigma^{(0)}_0(\omega) = N_f\int_{-\infty}^{\infty}d\varepsilon\, f(\varepsilon)|V(\varepsilon)|^2 G^{(1)}_0(\omega+\varepsilon)+\cdots, \tag{A14}$$

$$\Sigma_0^{(1)}(\omega)=\int_{-\infty}^{\infty}d\varepsilon\, f(-\varepsilon)|V(\varepsilon)|^2G_0^{(0)}(\omega-\varepsilon)$$
$$+(N_f-1)\int_{-\infty}^{\infty}d\varepsilon\, f(\varepsilon)|V(\varepsilon)|^2$$
$$\times G_0^{(2)}(\omega+\varepsilon)+\cdots, \tag{A15}$$

$$\Sigma_0^{(2)}(\omega)=2\int_{-\infty}^{\infty}d\varepsilon\, f(-\varepsilon)|V(\varepsilon)|^2$$
$$\times G^{(1)}(\omega-\varepsilon)+\cdots, \tag{A16}$$

where $f(\varepsilon)$ is the Fermi distribution function. Notice that a configuration with *m f* electrons can couple to the *m+1* configurations in N_f-m ways, but to the *m−1* configurations only in *m* ways. In the heavy-fermion regime the energy scale N_fV^2 is of the same magnitude as the other energy scales of the system (ε_f and *U*), which makes it possible to arrange the perturbation series as a $1/N_f$ expansion. Typical N_fV^2 values are in the range 0.1–1 eV. Another ''natural'' expansion parameter that emerges from the above series is the ratio $N_fV^2/(U-\varepsilon_f)$, which for a *U* of 6 eV and ε_f values between -1 and -3 eV would be in the range from 1/3 to 1/50. Therefore, the two expansion parameters are generally of comparable magnitude.

A simple, self-consistent self-energy approximation is obtained from the above formulas by everywhere replacing the bare Green's functions $G_0^{(m)}$ by the dressed ones $G^{(m)}$. This is a direct generalization of the usual NCA to the finite-*U* case. Pruschke and Grewe have argued[31] that this is in general a rather crude approximation. The basic problem is that the leading error term in the f^0 self-energy,

$$\Delta\Sigma^{(0)}=N_f(N_f-1)\int_{-\infty}^{\infty}d\varepsilon\, d\varepsilon' f(\varepsilon)f(\varepsilon')|V(\varepsilon)|^2$$
$$\times|V(\varepsilon')|^2G_0^{(1)}(\omega+\varepsilon)G_0^{(2)}(\omega+\varepsilon+\varepsilon')$$
$$\times G^{(1)}(\omega+\varepsilon'), \tag{A17}$$

is of order $N_fV^2/(U-\varepsilon_f)$, thus making the approximation dubious for a considerable range of parameters. To ensure the correctness of the theory to first order in *both* $1/N_f$ and $N_fV^2/(U-\varepsilon_f)$ we need to consider the extended set of equations,

$$\Sigma^{(n)}(\omega)=\Sigma_{NC}^{(n)}(\omega)+\Sigma_{VC}^{(n)}(\omega), \tag{A18}$$

with *n* ranging from 0 to 2. Here the Σ_{NC} are the self-energies given by Eqs. (A14)–(A16) with the bare Green's functions replaced by the interacting ones, while the ''vertex correction terms'' Σ_{VC} are given by[31]

$$\Sigma_{VC}^{(0)}(\omega)=N_f(N_f-1)\int_{-\infty}^{\infty}d\varepsilon|V(\varepsilon)|^2f(\varepsilon)G^{(1)}(\omega+\varepsilon)$$
$$\times\int_{-\infty}^{\infty}d\varepsilon'|V(\varepsilon')|^2f(\varepsilon')G^{(2)}(\omega+\varepsilon+\varepsilon')$$
$$\times G^{(1)}(\omega+\varepsilon'), \tag{A19}$$

$$\Sigma_{VC}^{(1)}(\omega)=(N_f-1)\int_{-\infty}^{\infty}d\varepsilon|V(\varepsilon)|^2f(-\varepsilon)G^{(0)}(\omega-\varepsilon)$$
$$\times\int_{-\infty}^{\infty}d\varepsilon'|V(\varepsilon')|^2f(\varepsilon')G^{(2)}(\omega+\varepsilon')$$
$$\times G^{(1)}(\omega+\varepsilon'-\varepsilon)$$
$$+(N_f-1)\int_{-\infty}^{\infty}d\varepsilon|V(\varepsilon)|^2f(\varepsilon)G^{(2)}(\omega+\varepsilon)$$
$$\times\int_{-\infty}^{\infty}d\varepsilon'|V(\varepsilon')|^2f(-\varepsilon')G^{(0)}(\omega-\varepsilon')$$
$$\times G^{(1)}(\omega+\varepsilon-\varepsilon'), \tag{A20}$$

$$\Sigma_{VC}^{(2)}(\omega)=\int_{-\infty}^{\infty}d\varepsilon|V(\varepsilon)|^2f(-\varepsilon)G^{(1)}(\omega-\varepsilon)$$
$$\times\int_{-\infty}^{\infty}d\varepsilon'|V(\varepsilon')|^2f(-\varepsilon')G^{(0)}(\omega-\varepsilon-\varepsilon')$$
$$\times G^{(1)}(\omega-\varepsilon'). \tag{A21}$$

The leading error term in the f^0 self-energy is now of order $[N_fV^2/(U-\varepsilon_f)]^2$, while the leading error in the f^1 self-energy is still $\sim(1/N_f^2)$.

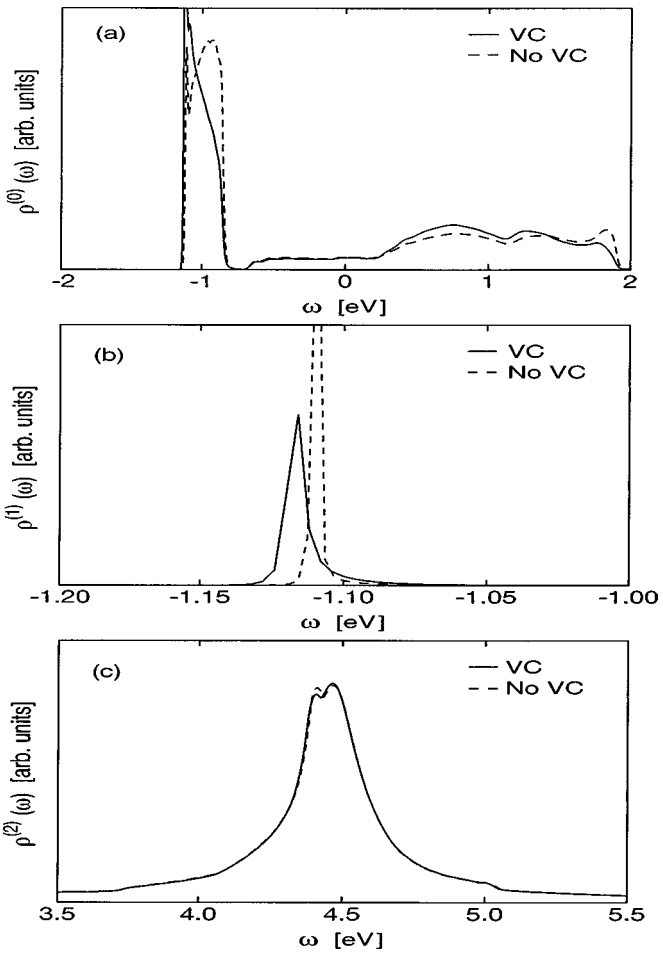

FIG. 14. Spectral functions for the f^0 (a), f^1 (b), and f^2 (c) configurations. Full lines display vertex corrected results, while dashed lines are calculated without vertex corrections.

As an example of the importance of the correction terms, we show in Fig. 14 the spectral functions for the different f configurations calculated with and without vertex corrections for a self-consistent CeP hybridization function. The position of the f level was $\varepsilon_f = -0.915$ eV. To simplify the numerics, the temperature was set at 60 K. The most important difference is that some of the f^0 weight is shifted down in energy when the vertex corrections are turned on, implying a larger f^0 component in the low-lying (thermally occupied) states of the system. In this case, the vertex corrections change the f^1 occupancy from 0.98 to 0.92, which will imply a considerable modification of the physical properties. Furthermore, the pole in the f^1 peak is broadened, and slightly shifted in energy. The f^2 spectrum, on the other hand, is largely unaffected by the corrections. This is consistent with the fact that the f^2 correction is of order $1/N_f^2$, and indicates that the $1/N_f$ expansion is converging rapidly.

It is remarkable that the treatment of the coupling to the f^2 configuration is so decisive in this case of relatively weak hybridization and high-lying ε_f. It shows, as previously discussed, that any *ab initio* theory of heavy-fermion systems must in some way take these couplings into account. Numerically this is, however, a difficult task due to the double integrals encountered in Eqs. (A19)–(A21), and the high accuracy needed near the sharp features of the spectra. A natural way of circumventing the problem is to work on a nonlinear (e.g., logarithmic) energy mesh that is dense around the peak structures but not elsewhere. This has the drawback that one needs to adjust the mesh for each iteration, which is cumbersome for a calculation like the present one, where the total number of iterations is large (since we have one self-consistency loop within another). Instead, we have chosen to work on a dense linear mesh (typically with a spacing of 1 meV), which allows us to do convolutions by fast Fourier transforms, so that the calculational time for the evaluation of the NCA self-energies scales as $N \ln N$ while the calculation of VC energies scales as $N^2 \ln N$, with N being the number of energy mesh points. With such a scheme, the NCA self-energies are easily evaluated, while the vertex corrections are still very time consuming. To arrive at a more manageable method, we simplify the form of the correction terms by ignoring the unimportant correction to the f^2 self-energy (A21), and by treating the integrals in the other terms by a coarse-graining procedure that relies on the fact that the spectral weights of the f^0 and f^1 configurations are concentrated in a region where the f^2 Green's function is relatively structureless. The basic idea is to replace the $G^{(2)}$ function by a suitable average g_2 that is then pulled outside the integrals. As an example, one could approximate the vertex correction to the f^0 and f^1 self-energies by

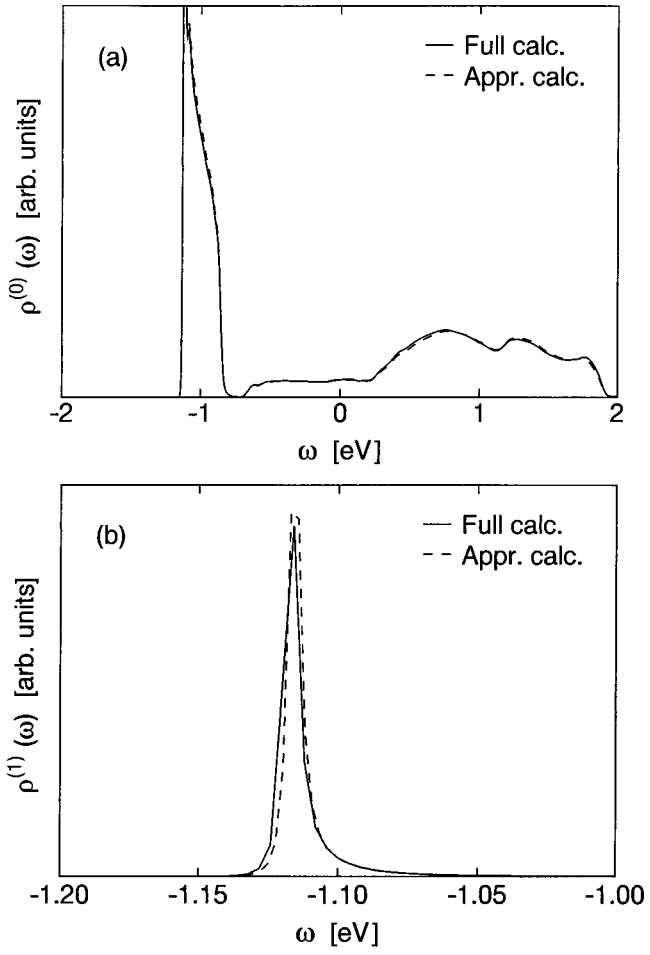

FIG. 15. Spectral functions for the f^0 (a) and f^1 (b) configurations. Full lines display fully vertex corrected results, while dashed lines are calculated with the coarse-graining approximation described in the text.

$$\Sigma_{VC}^{(0)}(\omega) = \Gamma_2(\omega) N_f (N_f - 1) \times \int_{-\infty}^{\infty} d\varepsilon |V(\varepsilon)|^2 f(\varepsilon) G^{(1)}(\omega + \varepsilon) \times \int_{-\infty}^{\infty} d\varepsilon' |V(\varepsilon')|^2 f(\varepsilon') G^{(1)}(\omega + \varepsilon') = \left(1 - \frac{1}{N_f}\right) \Gamma_2(\omega) \Sigma_{NCA}^{(0)}(\omega)^2, \tag{A22}$$

$$\Sigma_{VC}^{(1)}(\omega) = (N_f - 1) g_2(\omega) \int_{-\infty}^{\infty} d\varepsilon |V(\varepsilon)|^2 f(-\varepsilon) \times G^{(0)}(\omega - \varepsilon) \int_{-\infty}^{\infty} d\varepsilon' |V(\varepsilon')|^2 \times f(\varepsilon') G^{(1)}(\omega + \varepsilon' - \varepsilon) + (N_f - 1) g_2(\omega) \times \int_{-\infty}^{\infty} d\varepsilon |V(\varepsilon)|^2 f(\varepsilon) \int_{-\infty}^{\infty} d\varepsilon' |V(\varepsilon')|^2 \times f(-\varepsilon') G^{(0)}(\omega - \varepsilon') G^{(1)}(\omega + \varepsilon - \varepsilon') = 2\left(1 - \frac{1}{N_f}\right) g_2(\omega) \int_{-\infty}^{\infty} d\varepsilon |V(\varepsilon)|^2 \times f(-\varepsilon) G^{(0)}(\omega - \varepsilon) \Sigma_{NCA}^{(0)}(\omega - \varepsilon), \tag{A23}$$

with

$$g_2(\omega)=\frac{1}{\Delta}\int_{-\infty}^{\infty}d\varepsilon|V(\varepsilon)|^2 f(\varepsilon)G^{(2)}(\omega+\varepsilon), \quad \text{(A24)}$$

$$\Gamma_2(\omega)=\frac{1}{\Delta}\int_{-\infty}^{\infty}d\varepsilon|V(\varepsilon)|^2 f(\varepsilon)g_2(\omega+\varepsilon), \quad \text{(A25)}$$

$$\Delta=\int_{-\infty}^{\infty}d\varepsilon|V(\varepsilon)|^2 f(\varepsilon). \quad \text{(A26)}$$

These expressions can be evaluated by $N\ln N$ operations only. In our actual calculations we have refined the above approximation slightly by taking into account that the imaginary part of $G^{(1)}$ is almost a δ function while the real part samples a larger energy region, so that different averages of the $G^{(2)}$ function should be used for the different terms of the product of NCA self-energies. In Fig. 15 we show the configurational spectra calculated from this approximation together with the fully corrected ones. Parameters are the same as in Fig. 14. The curves are now almost indistinguishable over the whole energy range. Although this result is very encouraging, we emphasize that the coarse-graining procedure discussed here cannot be expected to be justified for all relevant parameters of the impurity model. In particular, one would expect it to become dubious in cases where the low-energy states have a significant f^2 component. This is, however, not the case for the models discussed in the present work.

Finally, we comment briefly on the evaluation of the physical Green's function. By a procedure similar to the one used for the partition sum, one can derive the general formula[41]

$$G_f(\omega)=\frac{1}{2\pi i}\oint_C dz\, e^{-\beta z}\mathrm{Tr}\left(\frac{1}{z-\hat{H}}\hat{f}^\dagger\frac{1}{z-\omega-\hat{H}}\hat{f}-\frac{1}{z-\omega-\hat{H}}\hat{f}^\dagger\frac{1}{z-\hat{H}}\hat{f}\right). \quad \text{(A27)}$$

Here C is a contour surrounding the poles of the resolvent operators, while the variable ω is assumed to carry an infinitesimal imaginary part yet still lying outside the contour C. Doing a simple NCA-like approximation one can derive the following equation for the spectral function:[5]

$$\rho_f(\omega)=\frac{1}{Z_f}\int_{-\infty}^{\infty}d\varepsilon\, e^{-\beta\varepsilon}(\rho^{(1)}(\varepsilon)\rho^{(0)}(\varepsilon-\omega)+(N_f-1)[\rho^{(2)}(\varepsilon)\rho^{(1)}(\varepsilon-\omega)+\rho^{(0)}(\varepsilon)\rho^{(1)}(\varepsilon+\omega)+\rho^{(1)}(\varepsilon)\rho^{(2)}(\varepsilon+\omega)]). \quad \text{(A28)}$$

In the infinite-U limit, this expression is correct to first order in $1/N_f$. For finite-U values there are correction terms of order N_fV^2/U, but the expression still gives the correct occupation numbers, as one can derive directly from Eqs. (A28) and (A7). As it turns out, the vertex corrections to Eq. (A28) are more difficult to evaluate in an economical manner than the corrections to the self-energies, so we have chosen to omit them in the present work. Thus, the vertex corrections enter in the evaluation of the configurational spectra, but not in the subsequent calculation of the physical Green's function from the configurational ones.

[1] The first experimental observation of heavy-fermion behavior was reported in K. Andres, J. E. Graebner, and H. R. Ott, Phys. Rev. Lett. **35**, 1779 (1975); For a review, see, e.g., P. Fulde, J. Keller, and G. Zwicknagl, in *Solid State Physics*, edited by H. Ehrenreich and D. Turnbull (Academic, New York, 1988), Vol. 41, p. 1; G. R. Stewart, Rev. Mod. Phys. **56**, 755 (1984).

[2] E. K. R. Runge, R. C. Albers, N. E. Christensen, and G. E. Zwicknagl, Phys. Rev. B **51**, 10 375 (1995); C. S. Wang, M. R. Norman, R. C. Albers, A. M. Boring, W. E. Pickett, H. Krakauer, and N. E. Christensen, *ibid.* **35**, 7260 (1987).

[3] P. W. Anderson, Phys. Rev. **124**, 41 (1961).

[4] O. Gunnarsson and K. Schönhammer, Phys. Rev. B **28**, 4315 (1983); *ibid.* **31**, 4815 (1985).

[5] N. E. Bickers, D. L. Cox, and J. W. Wilkins, Phys. Rev. B **36**, 2036 (1986).

[6] H. Kumigashira, S.-H. Yang, T. Yokoya, A. Chainani, T. Takahashi, A. Uesawa, and T. Suzuki, Phys. Rev. B **55**, R3355 (1997).

[7] A. J. Arko *et al.*, Phys. Rev. B **56**, R7041 (1997).

[8] A. Delin, P. M. Oppeneer, M. S. S. Brooks, T. Kraft, J. M. Wills, B. Johansson, and O. Eriksson, Phys. Rev. B **55**, R10 173 (1997).

[9] L. Z. Liu, J. W. Allen, O. Gunnarsson, N. E. Christensen, and O. K. Andersen, Phys. Rev. B **45**, 8934 (1992); J. W. Allen and L. Z. Liu, *ibid.* **46**, 5047 (1992).

[10] J. E. Han, M. Alouani, and D. L. Cox, Phys. Rev. Lett. **78**, 939 (1997).

[11] J.-S. Kang *et al.*, Phys. Rev. B **41**, 6610 (1990); O. Gunnarsson, N. E. Christensen, and O. K. Andersen, J. Magn. Magn. Mater. **76&77**, 30 (1988).

[12] G. Treglia, F. Ducastelle, and D. Spanjaard, J. Phys. (Paris) **41**, 281 (1980); **43**, 341 (1982).

[13] A. Georges and G. Kotliar, Phys. Rev. B **45**, 6479 (1992); M. Jarrell, Phys. Rev. Lett. **69**, 168 (1992).

[14] A. Georges, G. Kotliar, W. Krauth, and M. J. Rozenberg, Rev. Mod. Phys. **68**, 13 (1996), and references therein.

[15] W. Metzner and D. Vollhardt, Phys. Rev. Lett. **62**, 324 (1989); E. Müller-Hartmann, Z. Phys. B **74**, 507 (1989).

[16] H. Schweitzer and G. Czycholl, Z. Phys. B **83**, 93 (1991).

[17] M. M. Steiner, R. C. Albers, and L. J. Sham, Phys. Rev. B **45**, 13 272 (1992).

[18] H. Kajueter, G. Kotliar, and G. Moeller, Phys. Rev. B **53**, 16 214 (1996); G. Kotliar and H. Kajueter, *ibid.* **54**, R14 221 (1996); H. Kajueter and G. Kotliar, Int. J. Mod. Phys. B **11**, 729 (1997).

[19] V. I. Anisimov, A. I. Poteryaev, M. A. Korotin, A. O. Anokhin, and G. Kotliar, J. Phys.: Condens. Matter **9**, 7359 (1997).

[20] T. Suzuki *et al.*, Physica B **206-207**, 771 (1995); T. Suzuki, *ibid.* **186-188**, 347 (1993).

[21] A. Svane, Z. Szotek, W. M. Temmerman, J. Lægsgaard, and H.

Winter, J. Phys.: Condens. Matter **110**, 5309 (1998).
[22] W. Gudat, R. Rosei, J. H. Weaver, E. Kaldis, and F. Hulliger, Solid State Commun. **41**, 37 (1982).
[23] Y. Baer, R. Hauger, Ch. Zürcher, M. Campagna, and G. K. Wertheim, Phys. Rev. B **18**, 4433 (1978).
[24] F. Patthey, S. Cattarinussi, W.-D. Schneider, Y. Baer, and B. Delley, Europhys. Lett. **2**, 883 (1986).
[25] W.-D. Schneider, B. Delley, E. Wuilloud, J.-M. Imer, and Y. Baer, Phys. Rev. B **32**, 6819 (1985).
[26] A. Franciosi, J. H. Weaver, Nils Mårtensson, and M. Croft, Phys. Rev. B **24**, 3651 (1981).
[27] J. R. Schrieffer, *Theory of Superconductivity* (Addison-Wesley, Reading, Massachusetts, 1964).
[28] C. Calandra and F. Manghi, Phys. Rev. B **50**, 2061 (1994); F. Manghi, C. Calandra, and S. Ossicini, Phys. Rev. Lett. **73**, 3129 (1994).
[29] J. Lægsgaard, and A. Svane, Phys. Rev. B **55**, 4138 (1997).
[30] J. C. Slater and G. F. Koster, Phys. Rev. **94**, 1498 (1954).
[31] T. Pruschke and N. Grewe, Z. Phys. B **74**, 439 (1989).
[32] R. O. Jones and O. Gunnarsson, Rev. Mod. Phys. **61**, 689 (1989).
[33] O. K. Andersen, Phys. Rev. B **12**, 3060 (1975).
[34] H. L. Skriver, *The LMTO Method* (Springer-Verlag, Berlin, 1984).
[35] J. P. Perdew and A. Zunger, Phys. Rev. B **23**, 5048 (1981).
[36] R. W. G. Wyckoff, *Crystal Structures* (Wiley, New York, 1964), Vol. I.
[37] O. K. Andersen, O. Jepsen, and D. Glötzl, in *Canonical Description of the Band Structures of Metals*, Proceedings of the International School of Physics ''Enrico Fermi,'' Course LXXXIX, Varenna, 1985, edited by F. Bassani, F. Fumi, and M. P. Tosi (North-Holland, Amsterdam, 1985), p. 59.
[38] Ph. Lambin and J. P. Vigneron, Phys. Rev. B **29**, 3430 (1984).
[39] N. Takeda *et al.*, Physica B **186-188**, 153 (1993).
[40] O. Gunnarsson and O. Jepsen, Phys. Rev. B **38**, 3568 (1988).
[41] H. Keiter and G. Morandi, Phys. Rep. **5**, 227 (1984).